UNIVERSITÀ POLITECNICA DELLE MARCHE
SCUOLA DI DOTTORATO DI RICERCA IN SCIENZE DELL'INGEGNERIA
CURRICULUM IN INGEGNERIA MECCANICA

Elasto-dynamic modeling of a parallel kinematic robot with flexible links

Ph.D. Dissertation of:
Stefano Brillarelli

Advisor:
Prof. Matteo-Claudio Palpacelli

Curriculum Supervisor:
Prof. Giovanni Di Nicola

XXXIV edition - new series

UNIVERSITÀ POLITECNICA DELLE MARCHE
SCUOLA DI DOTTORATO DI RICERCA IN SCIENZE DELL'INGEGNERIA
CURRICULUM IN INGEGNERIA MECCANICA

Elasto-dynamic modeling of a parallel kinematic robot with flexible links

Ph.D. Dissertation of:
Stefano Brillarelli

Advisor:
Prof. Matteo-Claudio Palpacelli

Curriculum Supervisor:
Prof. Giovanni Di Nicola

XXXIV edition - new series

UNIVERSITÀ POLITECNICA DELLE MARCHE
SCUOLA DI DOTTORATO DI RICERCA IN SCIENZE DELL'INGEGNERIA
FACOLTÀ DI INGEGNERIA
Via Brecce Bianche – 60131 Ancona (AN), Italy

Acknowledgments

I would like to express my gratitude to my advisor, Prof. Ing. Matteo-Claudio Palpacelli, whose expertise and understanding, added considerably to my experience. I would also like to thank the Mechanical Engineering Group who followed me during my PhD program.
A very special thanks goes to my mother Paola and my father Desiderio who supported me throughout my study path, also a special thanks goes to my aunt Maria.

Ancona, Ottobre 2021

Stefano Brillarelli

Sommario

Il settore industriale negli ultimi anni sta vivendo una radicale trasformazione legata alle nuove esigenze del mercato. In risposta a queste ultime, la robotica sta proponendo da una parte soluzioni collaborative in modo da rendere più rapida l'installazione dei robot semplificandone la programmazione e la messa in opera e consentendo una interazione uomo-macchina, dall'altra sta affinando le prestazioni dei robot più propriamente industriali in modo da renderli sempre più veloci e accurati. In questo secondo ambito, la versatilità e la rapidità di risposta al mercato richiesta ai produttori alimenta quindi la ricerca di soluzioni tecniche orientate alla riduzione dei tempi ciclo con conseguente contenimento dei costi di produzione.

I materiali, le taglie dei motori elettrici utilizzati, le architetture cinematiche e le scelte progettuali in genere sono fattori importanti che incidono sulle prestazioni dinamiche dei robot. Ben noto è l'esempio dei robot a cinematica parallela utilizzati in numerosi settori per le elevate accelerazioni e velocità di esercizio che sono in grado di sviluppare. L'alleggerimento delle parti meccaniche in movimento consente una riduzione delle inerzie in modo da aumentare i range di velocità e accelerazione raggiungibili. Queste scelte meccaniche comportano l'insorgere di risposte dinamiche indesiderate, legate alla maggiore incidenza della flessibilità nella dinamica delle macchine.

Il presente lavoro è focalizzato sulla dinamica dei meccanismi a cinematica parallela nell'ipotesi che alcuni membri, resi più leggeri con una riduzione dello spessore dei profili meccanici, siano soggetti a deformazione elastica. La loro cedevolezza determina infatti errori nell'inseguimento di traiettoria oltre che differenti comportamenti nella stabilizzazione di posa all'inizio e alla fine del movimento assegnato.

Nel presente lavoro verranno presentati dei modelli dinamici per i link flessibili dei robot, i quali verranno utilizzati per la creazione di due modelli elasto-dinamici di robot a cinematica parallela a due gradi di libertà. Nel primo modello verrà applicata la Formulazione Aumentata di Lagrange nella ricerca delle relative equazioni del moto, mentre nel secondo verrà impiegato il Principio dei Lavori Virtuali con un set di parametri minimo.

Un modello ottimale deve infatti fornire le informazioni sulla dinamica flessibile di un robot nella maniera più efficiente possibile dal punto di vista computazionale. Tale criterio ha orientato la scelta del modello più promettente in termini di tempo di calcolo.

La scelta dei parametri fisici e geometrici del robot preso come esempio per lo

studio è stata trattata nel dettaglio considerando le problematiche che si possono verificare nel caso dell'allestimento di un banco prova, dove si suppone che la posizione dell'end effector venga acquisita con un sistema di visione.

I parametri geometrici hanno certamente una influenza sia sui modi di vibrare dei link flessibili che sulla geometria e dimensione dello spazio di lavoro: questi sono stati scelti in modo da far cadere le prime tre frequenze naturali delle aste all'interno di un range assegnato, in linea con la strumentazione disponibile nel laboratorio di Meccatronica e Robotica Industriale (MIR) dell'Università Politecnica delle Marche.

Il modello scelto è stato prima verificato tramite un modello agli elementi finiti e poi analizzato nel dettaglio. In particolare, è stato possibile ricavare delle mappe di cedevolezza, le quali hanno evidenziato le regioni dello spazio di lavoro del robot a maggiore cedevolezza, così che il progettista ne possa tenere conto in fase di progettazione e durante la fase di pianificazione dei task. É stato infine valutata l'efficienza computazionale del modello mettendolo a confronto con altri ottenuti per via numerica e per via software, da cui emergono le possibilità di implementazione dello stesso in algoritmi di controllo basati sul modello.

Abstract

In recent years, the industrial sector has undergone a radical transformation linked to new market needs. In response to the latter, robotics is proposing, on the one hand, collaborative solutions in order to speed up the installation of robots, simplifying their programming and implementation and allowing human-machine interaction, and, on the other hand, it is refining the performances of industrial robots in order to make them faster and more accurate. In this second area, the versatility and rapidity of response to the market feeds the manufacturers' search for technical solutions oriented to the reduction of cycle times with consequent containment of production costs.

The materials, the sizes of the electric motors used, the kinematic architectures and the design choices in general are important factors that affect the dynamic performance of robots. The example of parallel kinematic robots is well known and is used in many sectors for the high accelerations and operating speeds that they are able to develop. The lightening of their moving mechanical parts allows a reduction of the inertia in order to increase the speed and acceleration ranges that they can reach. These mechanical choices lead to the onset of undesirable dynamic responses, related to the greater incidence of flexibility in the dynamics of the machines.

The present work is focused on the dynamics of Parallel Kinematic Mechanisms (PKMs) under the hypothesis that some members, made lighter by reducing the thickness of their mechanical profiles, are subject to elastic deformation. In fact, their compliance determines errors in trajectory tracking as well as different behaviors in the stabilization of pose at the beginning and at the end of the assigned movement.

In the present work, dynamic models for flexible robot links will be presented and used to create two elasto-dynamic models of robots with parallel kinematics with two degrees of freedom. In the first model, the Augmented Lagrange Formulation will be applied in the search for the relevant equations of motion, while in the second, the Principle of Virtual Works with a minimum set of parameters will be employed.

In fact, an optimal model must provide the information about the flexible dynamics of a robot in the most computationally efficient way. This criterion guided the choice of the most promising model in terms of computational time.

The choice of the physical and geometrical parameters of the robot taken as an example for the study has been treated in detail considering the problems that may occur in the case of the setup of a test bench, where it is assumed that the position of the end effector is acquired with a vision system.

Geometrical parameters certainly have an influence both on the vibration modes of

the flexible links and on the geometry and size of the working space: these have been chosen so that the first three natural frequencies of the rods fall within an assigned range, in line with the instrumentation available in the laboratory of Mechatronics and Industrial Robotics (MIR) of the Polytechnic University of Marche.

The chosen model has been first verified by means of a finite element model and then analyzed in detail. In particular, it has been possible to derive compliance maps, which highlighted the regions of the robot workspace with higher compliant behaviour so that the designer could take them into account during the design phase and during the task planning phase. Finally, the computational efficiency of the model has been evaluated by comparing it with others obtained numerically and via software, from which the possibilities of implementing it in model-based control algorithms emerge.

Contents

List of Figures

List of Tables

Chapter 1.

Introduction

1.1. Motivation

One of the main reasons for the well-being that the most developed countries are experiencing today is the relative low cost that consumer goods have achieved in the industrial age. Despite the progressive increase in the price of materials, which is affected by the scarcity of resources at a global level, the technological evolution in the automation and robotics sector has made it possible to reduce production costs and at the same time increase product quality. Industrial robots have certainly played a central role in this evolutionary process, allowing an ever higher level of flexibility to meet the demand for smaller production batches.

Both serial and parallel robots are now widespread in the most varied sectors, integrated in workcells for palletizing, for the enslavement of CNC machines, for handling in general. They have pros and cons related to their intrinsic characteristics, that make them suitable for different functions.

The advantage of using robots in manufacturing processes is related to their ability to perform continuously and without loss of performance tasks that would be particularly tiring for a human operator.

Accuracy and repeatability represent two important parameters that define the effectiveness of a robot in performing a certain operation. In particular, the latter has a greater impact on the choice of the robot. It is the maximum error made by the robot in returning to a previously programmed position, whereas accuracy is the error or the difference between the desired position and the one that actually took place.

These parameters are mainly affected by three sources of error: the first one, which has also a greater impact on the positioning of a robot end-effector, concerns control of motors, the second is represented by the compliance of joints. Typically, it is of lesser entity if compared with the former. The last one, which has the least impact compared to the others, is represented by the compliance of members. Obviously, machining tolerances induce further inaccuracies in mechanics, but the latter can be evaluated and corrected by means of a calibration procedure.

Presently, the industrial trend is oriented towards two mainstreams: on the one hand, applications in which robots work alongside with the operator by cooperating in

various tasks, or more technically called applications *collaborative robotics* by means of *cobots*, on the other hand, fast applications where the fundamental interest is the reduction of the cost of production, which can be achieved by reducing the production time while ensuring the same quality level.

An in-depth analysis of the second target reveals that, in order to carry out a task more and more quickly, an increase of torque values or conversely a lightening of robot links is required in order to move the robot end-effector faster, sometimes using both solutions. These options lead to the onset of dynamic phenomena that determine a worsening of repeatability and accuracy with a consequent decline in the performance of the robot in trajectory tracking.

In collaborative and soft robotics, the speed of robots cannot be high for obvious reasons but, at the same time, there is a tendency to decrease their link masses by thinning the thickness of their mechanical parts or to reduce the latter mechanical stiffness, in order to prevent injuries of operators when a robot accidentally hits them during a task execution.

Therefore, an investigation and study of these aspects has the aim of improving the operating conditions of a widespread type of robots, quantifying and taking into account their incidence in the design of a robot and its controller.

1.2. State of art

Early research on the study and control of robots with flexible links dates back to the seventies. Research on this topic was encouraged and guided by two sectors: Industry and Space.

The former was mainly focused on increasing the dynamic performance of robots, namely high velocity and acceleration, providing them with a light mechanics and a resulting low inertia in order to reduce the cycle time of industrial operations and improve their productivity. Analogously, the weight of the equipment is a main determinant in the success of space expeditions, because cost is proportional to mass in such field. Therefore robots with high reaches must have a slight and slender mechanics.

Winfrey is one of the first authors to have addressed the flexibility in robot dynamics [1, 2], motivated by the fact that lighter and more slender robots are more subject to elastic deformation. He studied the deflection of the links of a four-bar mechanism working at high speed. Moreover, a couple of years later Book in his Ph.D. dissertation [3] began to deal with the topic of flexible robotics, proposing in the following period many other works [4–6]. In particular in [6], a recursive approach is described for writing the dynamics of robots with flexible links, which are assumed to have small displacements during operation.

In the aerospace sector, the first contributions related to the vibration control of dynamic systems can be found in [7], in which a feasibility analysis is made regarding

an active damping system that acts on a robot in order to attenuate the vibrations associated with the handling of a payload. Krishnamurthy and Chao [8] presented a dynamic model of two cooperating manipulators with the same kinematic structure based on two flexible links with two revolute joints and a rigid link grasped by the two end-effectors in a closed kinematic scheme. For other studies concerning these issues the scientific literature offers many other readings: Cyril et al. [9], Gouliaev and Zarrazhina [10], who studied flexible manipulators used for space applications, whereas a control method that uses input shaping was presented by Swada [11] in order to eliminate the vibrations acting on the arms of manipulators.

Another field in which flexible robotics found application is nuclear power plants, in particular many examples can be cited: concerning the storage of waste, Jansen [12] studied a long-reach-manipulation system for waste storage tank remediation and Kress [13] dealt with the modeling and control of a waste tank cleanup manipulator. Recently, Dubus, David and Measson [14] have investigated the application of a long reach elastic link inspection robot for the International Thermonuclear Experimental Reactor (ITER).

Another application in which aspects of flexible robotics are investigated is reported by Lin and Fu [15] and Chang and Fu [16], who analyzed a flexible manipulation system for automated deburring operation; in addition, the study of the dynamics of machines moving at high speed was treated using finite element models by Yang and Sadler [17] and Imdad Imam [18].

1.2.1. Serial Kinematic Machines (SKMs)

It can be noted from the mentioned works that their authors divided themselves into the study of flexible manipulators with serial or parallel kinematics.

Among the many studies in the literature, Oakley [19] presents a model for a 2R robot with a mass at the proximal end that acts as a payload and presents also the design of a non-linear controller for vibration suppression. In this study the proximal link is considered rigid whereas the distal one is considered flexible; in particular, the deformation of such link is modeled using the modal superposition, which will be addressed deeply in the following of the present work. Analogously, De Luca and Siciliano [20, 21] present a model for a 2R serial robot using the Assume Mode Method to model the deformation of the robot links, but unlike Oakley, they assume a flexibility for both robot links.

Many other works on the topic are proposed, such as the one of Paden et al. [22], who use finite element formulation for the modeling of the link deformation, whereas a work about an algorithm to solve the inverse dynamics of a 2R robot with both flexible links is proposed by Asada [23].

1.2.2. Parallel Kinematics Machines (PKMs)

Although most of the authors have worked on mechanisms with serial kinematics, several studies on parallel kinematics machines are available in the literature, albeit to a lesser extent: in particular one of the first studies presented, as previously mentioned, is the one of Winfrey and Imdad [18,24], who focused their study on a four-bar mechanism subject to dynamic loads because of the high speed. A further study by Turcic [25] presents a study on a four-bar mechanism in which the deformation of the links is modeled using a finite element formulation while the dynamics equations are obtained using the Lagrangian approach.

A work on a more complex manipulator was presented by Gasparetto [26], in particular he presented a general model applied to a five-bar mechanism where all the links are flexible. Deformation is modeled using a finite element approach, while the equations of motion are obtained by means of the principle of virtual works.
A different approach was presented by Briot and Khalil in [27], where they wrote the elastodynamic equations of a flexible five-bar linkage by means of the Principle of Virtual Power.
Wang [28] presented an approach for modeling parallel kinematics manipulators through sub-structures, in particular the deformation of the members is modeled using a finite element approach and the equations of motion are determined through the Lagrange augmented formulation approach.

A method similar to that of Gasparetto was proposed by Vidoni [29], whereas Mahmoodi [30] proposed a work in which the shape functions associated to the flexible links are evaluated in such a way that they best represented the dynamic behavior of the system, expressed as a function of the payload mass ratio on flexible mass links. The dynamics equations of the manipulator were obtained using the Lagrange formulation, and the dynamic response of the manipulator, whose model is obtained by superimposing different shape functions, is compared with a FEM model.

1.2.3. Modeling techniques

Another relevant aspect in the study of flexible robotics, which has a direct connection with the different kinematic architecture of manipulators, is the availability of different methodologies aimed at modeling the deformation of flexible links. Focusing on the most widespread approaches, they are: Assume Mode Method (AMM), Finite Element Method (FEM) and Lumped Parameter Method (LPM):

- The Assume Mode Method, which will be discussed in detail later, was used for example by Cannon [31], Chalhoub [32] and Siciliano [20]; this method establishes that the deformation of a flexible link associated to the dynamic effects is the sum of several suitably weighted functions; the latter are dependent on the links boundary conditions, namely how they are constrained at their ends. Since

each function corresponds to a way of vibrating and a finite number of modes is always used to approximate the link elastic behaviour, a problem can arise because an error is introduced in the deformation modeling due to the neglecting of high frequency modes of vibration. This effect, called *spillover*", was studied by Balas [33], who proposes a control algorithm as well as discussing its effects.

- The Finite Element Approach was used for example by Nagarajan [34], Tokhi [35], Theodore [36] and [37]. The latter compared it with the Assumed Modes Method. Regarding FEM, it was highlighted that the precision of the model is related to the number of elements in which the flexible links are divided, the increase of which also leads to an increase in the computational load, while regarding AMM, and/or to the degree of the shape functions [38]. This second approach is less common.

- Lumped Parameter Method was used for example by Zhu [39] and Khalil [40]. The main idea is a discretization of the flexible links by means of concentrated masses, which are connected to each other by means of springs and dampers.

The mentioned references represent only a small part of the works that can be found in the literature on flexible robotics; notably a major review was made by Dwivedy in 2006 [41].

1.2.4. Outline of the dissertation

In order to present this work in the most organic way, the following structure has been considered:

- *Chapter I* opens with the reasons that motivated this work and a section with the most relevant work at the state of the art. Cited works are organized both chronologically (based on human challenges in different periods) and by type of robot kinematic architecture, so that the reader can fully understand why some authors have moved towards certain approaches over others.

- *Chapter II* proposes two methodologies for modeling the deformation of the beam in small displacements. In particular, the use of Bézier polynomials is considered and compared with exact mathematical solutions. Strengths and weaknesses of each model have been highlighted in order to lay the foundation for a conscious choice of the most suitable modeling approach.

- *Chapter III* introduces the main concepts needed to develop elasto-dynamic models of parallel mechanisms. In particular, two general approaches are presented for modeling robots with flexible links. They are applied to two robots with a parallel kinematics and with two degrees of freedom. The first approach

that is presented exploits the Bézier polynomials to describe the deformation of the links, while the dynamics equations are obtained using Lagrange's augmented formulation; differently, the second approach allows to model the deformation of the links by means of the Assumed Modes Method, while the dynamics equations are obtained through the principle of virtual works. The chapter ends by choosing the most convenient approach in terms of efficiency so that an effective model of a parallel kinematics machine can be proposed and analysed.

- *Chapter IV* represents the heart of this work. In particular, an introductory section is focused on the writing of the elasto-dynamic model of a parallel kinematics manipulator two degrees of freedom. The chapter presents the values of its geometric parameters, explaining the reasons of the choices made. The work then continues by exposing the numerical simulation of this model, which is compared with the results an analogous simulation based on a Finite Element model. The last part of the chapter is dedicated to examining in detail the results obtained for the model, finally highlighting its strengths from the point of view of calculation time when compared to all the other models used in this work.

- *Chapter V* is the concluding chapter where results are summarized and some conclusions are drawn. Eventually, some suggestions for future research are given.

1.3. Contributions

Energy efficiency of machines, together with the need to maintain their performance at high levels in strategic sectors such as industrial, biomedical and space sectors, are orienting the scientific research towards systems capable of being more and more precise, performing, but also more light and flexible, to ensure operator safety and reduce consumption.

The concept of elaborating an elasto-dynamic model of a mechanism that, used in a control scheme, can improve its performance in terms of static and dynamic accuracy and repeatability goes in the direction shown above. One of the main difficulties encountered in modeling is the intrinsic complexity of dynamics of mechanical systems, especially when flexibility is taken into account. This work has tried to make this modeling easier and more efficient, providing a methodology specifically suited for parallel kinematics machines, although results are still preliminary and some improvements need to be made.

In addition, the issues addressed in this work can find application in industrial robotics, with companies that have in their product portfolio fast robots with slender arms and a parallel kinematics. Two well known examples can be found in Figure 1.1:

(a) FlexPicker **(b)** Delta robot

Figure 1.1.: Industrial robots with slender links. Courtesy of ABB (left) and Fanuc (right)

This work provides an integration to the basic theory of dynamics of continuous systems when it is applied to parallel kinematic machines, showing its advantages and disadvantages.

1.4. Publications arising from the research

- Carbonari, L, Brillarelli, S, Palpacelli, M, and Callegari, M., "Analysis of a Multibody Elastodynamic Model for Closed-Loop Kinematic Mechanisms". *Proceedings of the ASME 2019 International Design Engineering Technical Conferences and Computers and Information in Engineering Conference. Volume 9: 15th IEEE/ASME International Conference on Mechatronic and Embedded Systems and Applications*. Anaheim, California, USA. August 18–21, 2019.

- Brillarelli, S, and Palpacelli, M-C, "Design of a testbench for validating multibody flexible modeld aimed at reducing oscillations in parallel kinematic machines withflexible links". *Proceedings of the 2nd International Jc-IFToMM Symposium in conjunction with the 25th Symposium on Theory of Machines and Mechanisms*. Tokyo, Japan. October 25–26, 2019.

- Brillarelli, S, and Palpacelli, M-C, "An effective approach to model parallel robots with flexible links". *Proceedings of the 17th IEEE/ASME International Conference on Mechatronic and Embedded Systems and Applications (MESA), IDETC-CIE 2021 online conference.*. August 17–19, 2021.

Chapter 2.

Modeling of a flexible beam

Many approaches can be found in the literature to model the flexibility of links in compliant mechanical systems. In this section, two useful modeling tools are retrieved and compared.

2.1. Bézier curve in polynomial form

The first approach proposed to model the deformation of a flexible beam is based on the theory developed by Selig and Ding in [42] with the use of Bézier curves in polynomial form. Figure 2.1 shows some important geometrical details. Each cross section of the elastic beam can be localized by a reference frame attached to it with the origin coincident with its centroid. The x and y axes are aligned with the principal directions of the section. Each reference frame will be referred to a local reference frame $\{i\}$ located at the beginning of the beam.

The state of the flexible beam is described by means of a *deflection screw*, which represents a small displacement from the undeformed beam to its deformed configuration in terms of both rotation and translation elements: $\mathbf{s} = [\theta_x, \theta_y, \theta_z, v_x, v_y, v_z]^T$.

The deformation $\mathbf{s}(\mu, t)$ that a generic section of the beam undergoes is a function of both the distance μ from the origin of the reference frame $\{i\}$ along the undeformed middle axis of the beam, in this case the z axis, and time, according to the following

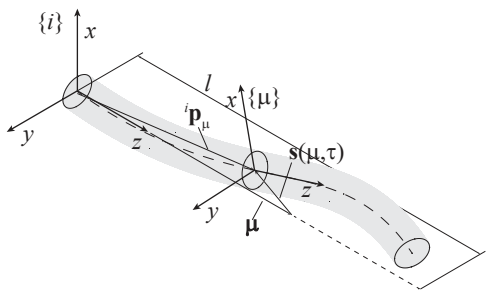

Figure 2.1.: Kinematic model of the flexible beam using a Bézier curve

equation written for a beam of unit length:

$$\mathbf{s}(\mu,t)=\sum_{i=0}^{n}\binom{n}{i}\mu^{i}(1-\mu)^{n-i}\mathbf{s}_{i}(t). \tag{2.1}$$

In equation (2.1), n represents the degree of the polynomial used and $\mathbf{s}_i(t)$ is the six-dimensional time dependent deflection screw related to the i^{th} degree of the polynomial. More explicitly, the expression of $\mathbf{s}(\mu,t)$ in (2.1) is valid only locally and for a beam of unit length. In order to expand this approach to a beam of any length, equation (2.1) has to be modified as follows:

$$\mathbf{s}(\mu,t)=\sum_{i=0}^{n}\frac{1}{(b-a)^{n}}\binom{n}{i}(\mu-a)^{i}(b-\mu)^{n-i}\mathbf{s}_{i}(t). \tag{2.2}$$

The expression shown above allows to define a Bézier curve from a, taken as the staring value along the undeformed beam, to b, considered as the final value. These assume the values $a=0$ and $b=l_f$ for a generic beam of length l_f. Since expression (2.1) represents the local deformation of the beam in local coordinates, a roto-translation is needed to describe the deformation with respect to a reference frame that lies on the beam end.

Using the same approach in [42], the required transformation has the form:

$${}^{0}\mathbf{s}=\mathbf{H}\,\mathbf{s}(\mu,t) \tag{2.3}$$

where matrixes $\mathbf{T}$ and $\mathbf{H}$ are defined as follows:

$$\mathbf{T}=\begin{bmatrix}0&-1&0\\1&0&0\\0&0&0\end{bmatrix},\quad \mathbf{H}=\begin{bmatrix}\mathbf{I}&\mathbf{0}\\\mu\mathbf{T}&\mathbf{I}\end{bmatrix}, \tag{2.4}$$

with $\mathbf{I}$ a 3×3 identity matrix and $\mathbf{0}$ a 3×3 null matrix with all zeros. After having defined the deformation function, the next step is the application of the kinematic congruence using the Timoshenko beam theory. A partial derivative of equation (2.2) provides:

$$\mathbf{s}'=\frac{d}{d\mu}\mathbf{s}+\mathbf{B}\mathbf{s}=\begin{pmatrix}\theta_x'\\\theta_y'\\\theta_z'\\v_x'-\theta_y\\v_y'+\theta_x\\v_z'\end{pmatrix}, \tag{2.5}$$

with $\mathbf{B}$ defined as:

$$\mathbf{B} = \begin{pmatrix} \mathbf{0} & \mathbf{0} \\ \mathbf{T} & \mathbf{0} \end{pmatrix}. \tag{2.6}$$

Said $\mathbf{k}$ a diagonal spring matrix for an infinitesimal slice of the beam, it has the form:

$$\mathbf{k} = \text{diag}(EJ_x, EJ_y, EJ_z, a_x GA, a_y GA, EA), \tag{2.7}$$

where E, A, J_i represent respectively the Young module, the cross section area of the beam and the area integrals, and a_x, a_y are constant scalars depending on the section shape. Moreover, $\mathbf{n}$ is the diagonal inertia matrix for unit of length:

$$\mathbf{n} = \rho\, \text{diag}(J_x, J_y, J_z, A, A, A), \tag{2.8}$$

where ρ is the density of the material.

It follows the expression of the *potential energy*:

$$E_p = \frac{1}{2} \int_0^{l_f} \mathbf{s'}^T \mathbf{k}\, \mathbf{s'}\, d\mu, \tag{2.9}$$

and the expression of the *kinetic energy*:

$$E_k = \frac{1}{2} \int_0^{l_f} \dot{\mathbf{s}}^T \mathbf{n}\, \dot{\mathbf{s}}\, d\mu. \tag{2.10}$$

Therefore, the Lagrangian function can be now written as:

$$\mathcal{L} = \frac{1}{2} \int_0^{l_f} (\dot{\mathbf{s}}^T \mathbf{n}\, \dot{\mathbf{s}} - \mathbf{s'}^T \mathbf{k}\, \mathbf{s'})\, d\mu. \tag{2.11}$$

From the Lagrangian function it is possible to derive the equations of motion. Said $\mathbf{k'}$ the following matrix:

$$\mathbf{k'} = -\mathbf{B}^T\, \mathbf{k} - \mathbf{k}\, \mathbf{B}, \tag{2.12}$$

the resulting dynamic equation is:

$$\mathbf{k}\mathbf{s''} + \mathbf{k'}\mathbf{s'} - n\ddot{\mathbf{s}} = \mathbf{0}. \tag{2.13}$$

As already demonstrated by many authors, the performance of this model are really influenced by the choice of the polynomial degree. In order to highlight this effect, a modal analysis of a beam can be presented as the degree of the polynomial varies. Equation (2.13) can be written in the form:

$$\mathbf{M}\ddot{\mathbf{s}} + \mathbf{K}\dot{\mathbf{s}} = \mathbf{0}, \tag{2.14}$$

so that the problem of finding the normal frequencies can be translated in a search of the eigenvalues of the dynamic matrix $\mathbf{A}$ defined as:

$$\mathbf{A} = \mathbf{M}^{-1}\mathbf{K}.$$

Such analysis is applied to a beam clamped at one end and free at the other end. All the geometrical parameter considered for the analysis are shown in table 2.1, while the natural flexural frequencies are shown in table 2.2.

Geometrical property			
length of beam	l	0.3	[m]
section parameter	b x h	10x0.5	[mm]
area integral	J_x	$\frac{b \times h^3}{12}$	[m^4]
area integral	J_y	$\frac{b \times h^3}{12}$	[m^4]
area integral	J_z	$\frac{b \times h^3}{12}$	[m^4]
section form factor	a_x	$\frac{2}{3}$	
Young modul	E	200	[GPa]

Table 2.1.: Values of the geometrical properties

Normal modes at increasing values of polynomial degree									
Frequencies		**I**	**II**	**III**	**IV**	**V**	**VI**	**VII**	**VIII**
Degree of polynomials	$n = 3$	11.843	2108						
	$n = 4$	6.189	79.59	3690.9					
	$n = 5$	5.231	36.659	5627.9					
	$n = 6$	4.955	31.28	100.18	563.6	7920.5			
	$n = 7$	4.82	30,338	84.548	198.15	1078.2	10570		
	$n = 8$	4.7414	29.808	83.327	162.22	339.01	1858.2	13579	
	$n = 9$	4.693	29.464	82.649	161.17	265.62	533.9	2976.1	16951

Table 2.2.: Values of the normal frequencies in [Hz]

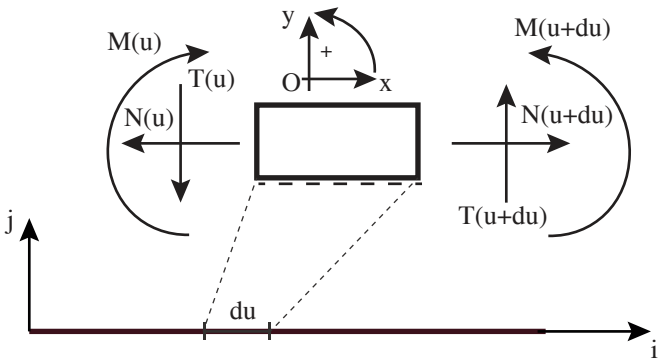

Figure 2.2.: Small segment of a flexible beam: internal force system

2.2. Assumed Modes Method

A second approach used in this work to model the dynamics of a flexible beam is the Assumed Modes Method [38]. The latter allows to discretize the beam, which is a distributed-parameter system, starting with the discretization of the boundary-value problem in an implicit manner. It is a method that gives the opportunity to formulate the forced response problem for a discretized system, rather than focusing only on its free response. Typically the equations of motion of a flexible beam derive from a Lagrangian approach. In the following, the idea of modeling the dynamic behaviour of a flexible beam by means of a linear combination of assumed funtions is inherited from the Assume Modes Theory.

2.2.1. Vibrating modes of a flexible beam

The response of a flexible beam in bending vibration can be found according to the following procedure. Called v the transverse displacement of a small segment along the y direction of the beam, as shown in Figure 2.2, the rotation equilibrium about the z axis and the translation equilibrium along the y axis provide:

$$+\circlearrowleft \qquad M(u+du) - M(u) + T(u+du)du = I_z \frac{\partial^2 v'}{\partial t^2} \tag{2.15}$$

$$+\uparrow \qquad T(u+du) - T(u) = \rho A du \frac{\partial^2 v}{\partial t^2} \tag{2.16}$$

where du is the infinitesimal segment along the middle axis of the beam, A is the area of the cross section, ρ is the density of the material, I_z is the cross-sectional area moment of inertia, T and M are the shearing force and the bending moment respectively, and $v' = \partial v / \partial u$ is the slope of the beam, where the operator $(')$ means a derivative over u. A development of both T and M expressions in (2.16) at the

$(u + du)$ section up to the first order provides:

$$M(u + du) = M(u) + \frac{\partial M(u)}{\partial u} du + ... \tag{2.17}$$

$$T(u + du) = T(u) + \frac{\partial T(u)}{\partial u} du + ... \tag{2.18}$$

Such expressions can be used in (2.16) to replace their corresponding terms so that:

$$+ \circlearrowleft \quad M(u) + \frac{\partial M(u)}{\partial u} du - M(u) + (T(u) + \frac{\partial T(u)}{\partial u} du) du = I_z \frac{d^2 v'}{dt^2} \tag{2.19}$$

$$+ \uparrow \quad T(u) + \frac{\partial T(u)}{\partial u} du - T(u) = \rho A du \frac{\partial^2 v}{\partial t^2} \tag{2.20}$$

Some assumptions are typically made in order to solve the previous equations [38]:

- small displacements are hypothesized;
- the axial load N shown in Figure 2.2 is neglected [1];
- the cross-sectional area moment of inertia I_z is neglected;
- the angular acceleration is neglected [2].

These assumptions lead to:

$$+ \circlearrowleft \quad \frac{\partial M(u)}{\partial u} du = -T(u) \tag{2.21}$$

$$+ \uparrow \quad T' = \rho A \frac{\partial^2 v}{\partial t^2} \tag{2.22}$$

As well-known from the mechanics of materials, curvature k in the hypothesis of small displacements is directly related to the moment according to the expression $M = EI\kappa$. It follows from (2.22) the partial differential equation for bending vibration of a beam:

$$-\frac{\partial^2 EI_z v''(u,t)}{\partial u^2} = \rho A \frac{\partial^2 v(u,t)}{\partial t^2}. \tag{2.23}$$

Equation (2.23) has to be solved applying the boundary conditions that depend on how the beam is constrained and on the type of loads. It can be solved separating the position variable u from time t as follows:

[1] in [43] this assumption is removed.

[2] a work where it's possible to see a model with this approach is [44].

$$v(u,t) = \sum_{i=1}^{\infty} \chi_i(u)\, \eta_i(t), \tag{2.24}$$

where $\chi_i(u)$ represents the modal form, while $\eta_i(t)$ is the harmonic function related to the i^{th} natural frequency. By combining (2.24) and (2.23) and considering a constant Young modulus and cross section for the beam, it follows:

$$-\frac{EI_z}{\rho A}\frac{1}{\chi_i(u)}\frac{d^4\chi_i(u)}{du^4} = \frac{\ddot{\eta}_i(t)}{\eta_i(t)} = \lambda. \tag{2.25}$$

in which the partial derivative has been replaced with the total derivative because χ depends only on u and η only on t. On the right of equation (2.25) it is easy to see that:

$$\ddot{\eta}(t) - \lambda\, \eta(t) = 0. \tag{2.26}$$

If $\lambda > 0$ then the two roots in (2.26) are all positive or one positive and one negative. A positive root means a divergent solution that can't be accepted in the hypothesis of small displacements, therefore It must be $\lambda < 0$. Further developments provide:

$$\lambda = -\omega^2 \tag{2.27}$$

$$s_{1,2} = \sqrt{\lambda} = \pm\, j\omega \tag{2.28}$$

$$\eta(t) = c_1 e^{j\omega t} + c_2 e^{-j\omega t} \tag{2.29}$$

From expression (2.25) it is also:

$$\lambda = -\omega_i^2 \tag{2.30}$$

$$-\frac{EI_z}{\rho A}\frac{1}{\chi_i(u)}\frac{d^2\chi_i(u)}{du^2} = \frac{\ddot{\eta}_i(t)}{\eta_i(t)} = -\omega_i^2 \tag{2.31}$$

$$-\frac{EI_z}{\rho A}\frac{1}{\chi_i(u)}\frac{d^4\chi_i(u)}{du^4} = -\omega_i^2 \tag{2.32}$$

By applying the substitution:

$$\beta^4 = \frac{\omega^2 \rho A}{EI_z}, \tag{2.33}$$

it is now possible to find the equation of the i^{th} modal form:

$$\frac{d^4\chi_i(u)}{du^4} - \beta_i^4\chi_i(u) = 0 \tag{2.34}$$

$$\chi_i(u) = a_0\sin(\beta_i u) + a_1\cos(\beta_i u) + a_2\sinh(\beta_i u) + a_3\cosh(\beta_i u) \tag{2.35}$$

2.2.2. Boundary conditions

In order to find the natural frequencies of beam clamped at one end and free to the other end, it is necessary to impose the corresponding boundary conditions. They are imposed to $\chi_i(u)$ as follows:

- null displacement at the clamped end: $\chi(0) = 0$
- null rotation at the clamped end: $\dfrac{d\chi(0)}{du} = 0$
- null bending moment at the free end: $EI_z\dfrac{d^2\chi(l)}{du^2} = 0$
- null shearing force at the free end: $-\dfrac{d}{du}EI_z\dfrac{d^2\chi(l)}{du^2} = 0$

With the first three conditions it is possible to find the three integration constants a_1, a_2, a_3. They are all functions of an integration constant a_0. The last condition allows to obtain the natural frequency of the system. In particular, the integration constant assumes the following values:

$$\begin{aligned} a_3 &= -a_1; \\ a_2 &= -a_0 \\ a_1 &= -\frac{a_0\,\sin(\beta\,l) + a_0\sinh(\beta\,l)}{\cos(\beta\,l) + \cosh(\beta\,l)} \end{aligned}$$

In (2.35) the three mentioned parameters can be replaced giving:

$$\begin{aligned} \chi_i(u) = a_0\Bigg[&\sin(\beta u) - \sinh(\beta u) - \cos(\beta u)\,\frac{\sin(\beta\,l) + \sinh(\beta\,l)}{\cos(\beta\,l) + \cosh(\beta\,l)} + \\ &+\cosh(\beta u)\,\frac{\sin(\beta\,l) + \sinh(\beta\,l)}{\cos(\beta\,l) + \cosh(\beta\,l)}\Bigg] \end{aligned} \tag{2.36}$$

Finally, imposing the last condition on the shearing force at the free end, the problem can be solved by finding the natural frequencies for a clamped beam, namely:

Normal modes				
$\beta\ [\mathrm{m}^{-1}]$	6.2503	15.6470	26.1827	36.6517
Frequencies [Hz]	4.544	28.479	79.743	156.262

Table 2.3.: Values of normal modes

$$\tilde{x} = \beta l$$
$$2\,E\,I_z\,\tilde{x}^3\,\frac{(\cos(\tilde{x})\,\cosh(\tilde{x})+1)}{l^3} = 0$$

where, for the first four natural frequencies in non-dimensional form it is:

$$\tilde{x}_1 = 1.8751$$
$$\tilde{x}_2 = 4.6941$$
$$\tilde{x}_3 = 7.8548$$
$$\tilde{x}_4 = 10.9955$$

In Figure 2.3 the trend of the first four modal shapes for a clamped beam is shown. In particular, with reference to a beam of the geometrical parameters gathered in Table 2.1, the natural frequencies assume the values shown in Table 2.3.

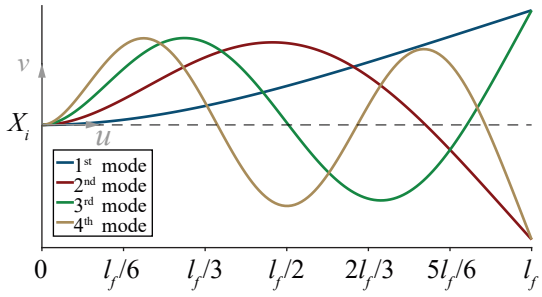

Figure 2.3.: Trend of the first four modes of a clamped beam

2.2.3. Damping model for a flexible beam

A more realistic model, which takes into account the natural dissipative effects of physical systems, can be defined by adding an internal damping to the flexible beam.

In fact a damping contribution implies a loss of energy during the motion of the beam, simulating the effect of microstructural defects, such as grain boundaries and impurities [45].

The Kelvin-Voigt model is used in this work to model the internal damping of the material. This model is well-known in the literature. The reader can find more examples of its application in [43, 44]. Starting from (2.23) and adding the mentioned viscous term, it can be obtained:

$$\rho A \frac{\partial^2 v}{\partial t^2} + \frac{\partial^2}{\partial u^2} C I_z \frac{\partial^2}{\partial u^2} \frac{\partial v}{\partial t} + \frac{\partial^2}{\partial u^2} E I_z \frac{\partial^2 v}{\partial u^2} = 0, \tag{2.37}$$

where C represents the viscous-elastic coefficient. This formulation has no effect on the value of the natural frequencies of the system. Equation (2.37), by means of (2.24) can be written again in the form:

$$\rho A \chi_i(u) \frac{\partial^2 \eta_i(t)}{\partial t^2} + \frac{\partial^4}{\partial u^4} \chi_i(u) C I_z \frac{\partial \eta_i(t)}{\partial t} + \frac{\partial^4}{\partial u^4} E I_z \chi_i(u) \eta_i(t) = 0$$

which can be arranged as follows:

$$-\frac{E I_z}{\rho A \chi(u)} \frac{\partial^4 \chi(u)}{\partial u^4} = \frac{\ddot{\eta_i}(t)}{\eta_i(t) + \frac{C}{E} \dot{\eta_i}(t)} = \omega_i^2$$

2.3. Comparison between the proposed models

Some differences can be highlighted between the two models proposed in this section, according to the theoretical material provided above. The assumed modes method approximates the behaviour of a flexible beam by narrowing its modal content to a certain order. High frequencies are usually neglected in favour of low frequencies, which certainly have the highest energy content. The former have a lesser impact than the latter in real deformations of a beam, because of more reduced amplitudes of the deformation at high frequencies and because of the internal damping of the material. A look at the data of Table 2.4, where the results of Table 2.2 are proposed again with the addition of a further row based on the exact solution of the mathematical model, reveals that a higher degree of the polynomial, equal or greater than the ninth grade, is needed in order to have a low error for the first two normal modes (in the order of 3%).

Normal modes at increasing values of polynomial degree									
Frequencies		**I**	**II**	**III**	**IV**	**V**	**VI**	**VII**	**VIII**
Polynomial degree	$n = 3$	11.843	2108						
	$n = 4$	6.189	79.59	3690.9					
	$n = 5$	5.231	36.659	5627.9					
	$n = 6$	4.955	31.28	100.18	563.6	7920.5			
	$n = 7$	4.82	30,338	84.548	198.15	1078.2	10570		
	$n = 8$	4.7414	29.808	83.327	162.22	339.01	1858.2	13579	
	$n = 9$	4.693	29.464	82.649	161.17	265.62	533.9	2976.1	16951
Exact solution		4.544	28.479	79.743	156.262	258.31	385.88	538.95	717.54

Table 2.4.: Normal frequencies in Hz

Chapter 3.

Formalization of the elasto-dynamic problem

The approaches discussed in the previous chapter to model flexible beams have been employed to develop two alternative models of a generic parallel kinematics robot, by respectively using the Augmented Lagrangian Formulation [46] and the Principle of Virtual Work [47]. The aforementioned approaches have been then followed to study a parallel robot with two degrees freedom and compare the performance of the adopted models in order to choose the most effective.

3.1. Elasto-dynamic model using Augmented Lagrange Formulation

Before using the beam deformation model based on Bézier curves in polynomial form, it is necessary to develop a general method to model the rigid and flexible links of a parallel kinematic robot; this approach can be also applied to serial robots once the appropriate considerations have been stated.

However, according to the literature, the most followed approach consists on the writing of the motion equations obtained by means of Augmented Lagrangian Formulation. As an example, Figure 3.1 shows a generic rigid beam in three-dimensional space, thus possessing six degree of freedom.

Here, vector $\mathbf{p}_0 = \left[x_0, y_0, z_0\right]^T$ expresses the position of the origin of frame $\{1\}$ with respect to base frame $\{0\}$; by using the Euler parameters, the relative orientation of the aforementioned frames is expressed by the following rotation matrix:

$$\mathbf{R}_{rig} = \begin{bmatrix} {e_0}^2 + {e_1}^2 - {e_2}^2 - {e_3}^2 & 2\,e_1\,e_2 - 2\,e_0\,e_3 & 2\,e_0\,e_2 + 2\,e_1\,e_3 \\ 2\,e_0\,e_3 + 2\,e_1\,e_2 & {e_0}^2 - {e_1}^2 + {e_2}^2 - {e_3}^2 & 2\,e_2\,e_3 - 2\,e_0\,e_1 \\ 2\,e_1\,e_3 - 2\,e_0\,e_2 & 2\,e_0\,e_1 + 2\,e_2\,e_3 & {e_0}^2 - {e_1}^2 - {e_2}^2 + {e_3}^2 \end{bmatrix} \tag{3.1}$$

By using equation (3.1), the position of the beam centre of mass P is computed as:

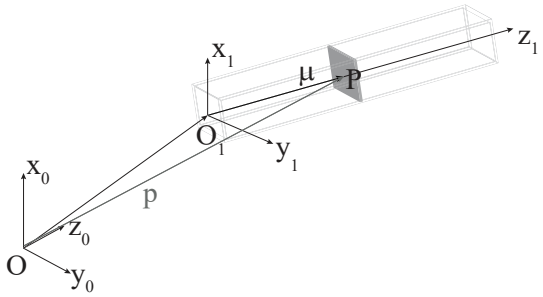

Figure 3.1.: A rigid beam in the space

$$\mathbf{p}_{cm} = \mathbf{p}_0 + \mathbf{R}_{rig} \begin{bmatrix} 0 \\ 0 \\ l/2 \end{bmatrix}$$

where l is the beam length. Once the centre of mass position has been calculated, its velocity can be expressed as:

$$\mathbf{v}_{cm} = \dot{\mathbf{p}}_0 + \mathbf{S}\mathbf{R}_{rig} \begin{bmatrix} 0 \\ 0 \\ l/2 \end{bmatrix}$$

where matrix $\mathbf{S}$ has the form:

$$\mathbf{S} = \begin{bmatrix} 0 & -\Omega_z & \Omega_y \\ \Omega_z & 0 & -\Omega_x \\ -\Omega_y & \Omega_x & 0 \end{bmatrix} = \mathbf{\Omega}\times$$

with $\mathbf{\Omega} = [\Omega_x, \Omega_y, \Omega_z]^T$ being the angular velocity vector. The beam kinetic and potential energy are then computed as a function of the centre of mass position and velocity:

$$T = \frac{1}{2}\mathbf{v}_{cm}^T m\, \mathbf{v}_{cm} + \frac{1}{2}\mathbf{\Omega}^T \mathbf{I}\, \mathbf{\Omega} \tag{3.2}$$

$$V = m\mathbf{g}^T \mathbf{p}_{cm} \tag{3.3}$$

where $\mathbf{g}$ is the gravity acceleration and $\mathbf{I}$ is the inertia matrix relative to the centre of mass of the beam.

In order to account for the beam flexibility, the contributions to kinetic and potential energy due to its deformation must be added to expression (3.2) and (3.3). As a matter of fact, and as a result of flexibility, the generic point P will no longer belong to the beam axis: on the contrary, it will be moved to position P', as shown by the displacement vector $\mathbf{s}$ in Figure 3.2.

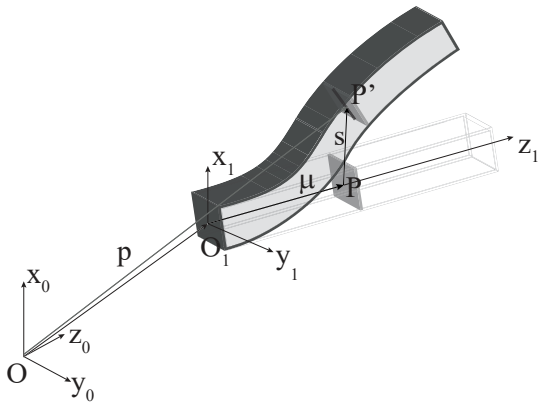

Figure 3.2.: A flexible beam in the space

Said s_x and s_y the displacements along the axis lying on the beam section, and s_z the displacement along a direction perpendicular to the beam section, the generic deformation expressed by using Bézier curves has already been derived in the previous section with the equation (2.2), presented here again:

$$\mathbf{s}(\mu, t) = \sum_{i=0}^{n} \frac{1}{(b-a)^n} \binom{n}{i} (\mu - a)^i (b - \mu)^{n-i} \mathbf{s}_i(t) \tag{3.4}$$

Therefore, the position of a generic point of the beam is computed as:

$$\mathbf{p}_p = \mathbf{p}_0 + \mathbf{R}_{rig} \left(\begin{bmatrix} 0 \\ 0 \\ \mu \end{bmatrix} + \begin{bmatrix} s_x \\ s_y \\ s_z \end{bmatrix} \right)$$

where μ is the distance of point P from the origin O_1 of frame $\{1\}$. The velocity of point P is then obtained as the derivative of the previous expression as a function of time:

$$\mathbf{v}_p = \dot{\mathbf{p}}_0 + \mathbf{S}\,\mathbf{R}_{rig} \begin{bmatrix} s_x \\ s_y \\ \mu + s_z \end{bmatrix} + \mathbf{R}_{rig} \begin{bmatrix} \dot{s}_x \\ \dot{s}_y \\ \dot{s}_z \end{bmatrix}$$

Moreover, the angular velocity $\boldsymbol{\omega}$ of a generic small segment of the beam is expressed as:

$$\boldsymbol{\omega} = \begin{bmatrix} \Omega_x + [1 \quad 0 \quad 0]\, \mathbf{R}_{rig}\boldsymbol{\theta}(\mu,t) \\ \Omega_y + [0 \quad 1 \quad 0]\, \mathbf{R}_{rig}\boldsymbol{\theta}(\mu,t) \\ \Omega_z + [0 \quad 0 \quad 1]\, \mathbf{R}_{rig}\boldsymbol{\theta}(\mu,t) \end{bmatrix}$$

with $\boldsymbol{\theta}(\mu,t) = [\theta_x(\mu,t), \theta_y(\mu,t), \theta_z(\mu,t)]^T$. The previous expressions can be written again in the following explicit and compact form:

$$\mathbf{s}_d = \begin{bmatrix} \Omega_x + [1 \quad 0 \quad 0]\, \mathbf{R}_{rig}\boldsymbol{\theta}(\mu,t) \\ \Omega_y + [0 \quad 1 \quad 0]\, \mathbf{R}_{rig}\boldsymbol{\theta}(\mu,t) \\ \Omega_z + [0 \quad 0 \quad 1]\, \mathbf{R}_{rig}\boldsymbol{\theta}(\mu,t) \\ \mathbf{v}_{px} \\ \mathbf{v}_{py} \\ \mathbf{v}_{pz} \end{bmatrix} \tag{3.5}$$

Finally, expression (3.5) can be exploited to compute the kinetic energy of the flexible beam:

$$T = \frac{1}{2}\mathbf{s}_d^T \begin{bmatrix} \mathbf{R}_{rig} & \mathbf{0} \\ \mathbf{0} & \mathbf{I} \end{bmatrix} \mathbf{N} \begin{bmatrix} \mathbf{R}_{rig} & \mathbf{0} \\ \mathbf{0} & \mathbf{I} \end{bmatrix} \mathbf{s}_d \tag{3.6}$$

where $\mathbf{N}$ is the beam mass matrix:

$$\mathbf{N} = \begin{pmatrix} J_x\,\rho & 0 & 0 & 0 & 0 & 0 \\ 0 & J_y\,\rho & 0 & 0 & 0 & 0 \\ 0 & 0 & J_z\,\rho & 0 & 0 & 0 \\ 0 & 0 & 0 & A\,\rho & 0 & 0 \\ 0 & 0 & 0 & 0 & A\,\rho & 0 \\ 0 & 0 & 0 & 0 & 0 & A\,\rho \end{pmatrix}$$

The mass matrix also contains the normalization equation of the Euler parameters, remembering that rotations have been modeled using a rotation matrix based on Euler parameters.

As stated before, the potential energy due to the flexibility of the beam, which has been discussed in Section 2.1, must be added to the gravitational energy expressed by (3.3); therefore the total potential energy is computed as:

$$V = m\mathbf{g}^T\mathbf{p}_{cm} + \frac{1}{2}\mathbf{s}'^T(\mu,t)\mathbf{K}\mathbf{s}'(\mu,t) \tag{3.7}$$

where $\mathbf{K}$ is the stiffness matrix per unit length:

$$\mathbf{K} = \text{diag}(EJ_x, EJ_y, EJ_z, a_xGA, a_yGA, EA) \tag{3.8}$$

The kinetic and potential energy of a generic robot composed by an assembly of n links can be simply computed as:

$$T = \sum_0^n T_i \tag{3.9}$$

$$V = \sum_0^n V_i \tag{3.10}$$

where T_i and V_i refer respectively to the kinetic and potential energy of the i^{th} link; here, expressions (3.2) and (3.3) are used if link i is rigid, whereas expressions (3.6) and (3.7) are used if link i is flexible. Once the robot kinetic and potential energy have been computed, the dynamic equations of motion can be derived through the Augmented Lagrangian Formulation:

$$\frac{d}{dt}\frac{\mathcal{L}}{d\dot{\mathbf{q}}} - \frac{\mathcal{L}}{d\mathbf{q}} - \mathbf{\Phi}_q^T\boldsymbol{\lambda} = \mathbf{f} \tag{3.11}$$

where $\mathbf{q}$ is the generalized coordinates vector that contains the rigid position and orientation parameters as well as the coefficients of the Bézier polynomial, which are related to the deformation parameters; finally, vector $\dot{\mathbf{q}}$ express the derivatives of $\mathbf{q}$ as a function of time.

Matrix $\mathbf{\Phi}_q$ expresses the constraints the system is subject to, whereas vector $\boldsymbol{\lambda}$ represents the generalized reaction forces necessary to comply with the kinematic constraints.

Equation (3.11) can be finally rewritten in the following form:

$$\begin{cases} \mathbf{M}\,\ddot{\mathbf{q}} + \mathbf{\Phi}_q^T\boldsymbol{\lambda} = -\mathbf{\Gamma}(\mathbf{q},\dot{\mathbf{q}}) \\ \mathbf{\Phi}_q\ddot{\mathbf{q}} = -\dot{\mathbf{\Phi}}_q\dot{\mathbf{q}} - \dot{\mathbf{\Phi}}_t \end{cases} \tag{3.12}$$

This vector equation should be modified to include terms that apply a stabilizing action during integration in order to monitor and regulate violations of position and velocity constraints; this approach, proposed by Baumgarte, consists in rewriting the

previous equation as follows:

$$\begin{bmatrix} \mathbf{M} & \mathbf{\Phi}_q^T \\ \mathbf{\Phi}_q & \mathbf{0} \end{bmatrix} \begin{bmatrix} \ddot{\mathbf{q}} \\ \boldsymbol{\lambda} \end{bmatrix} = \begin{bmatrix} -\mathbf{\Gamma}(\mathbf{q}, \dot{\mathbf{q}}) \\ -\dot{\mathbf{\Phi}}_q \dot{\mathbf{q}} - \dot{\mathbf{\Phi}}_t - 2\alpha \dot{\mathbf{\Phi}} - \beta^2 \mathbf{\Phi} \end{bmatrix} \tag{3.13}$$

where α and β respectively represent the coefficients that stabilize the position and speed errors. In equation (3.13) the values of λ clearly differ greatly from those calculated with (3.12), therefore such values are not reliable for the evaluation of the constraint reactions of the kinematic pairs.

3.1.1. An application of the model to a planar PKM with 2-DOFs

The model presented in the previous section can be used to study the planar parallel kinematic robot showed in the following figure. The system is composed of two flexible beams connected in point B through a revolute joint. A revolute joint also connects each beam to a rigid slider which is constrained on the robot frame by means of a prismatic joint. The two sliders, considered massless, move along rails arranged orthogonally with respect to each other.

According to the model presented in the previous section, the first step of the approximation method is the choice of the degree of the Bézier polynomial; here, a fifth degree polynomial formulation has been chosen, because it allows to minimize the error computed in the first modal frequency. Therefore, the expression of the polynomial given in (2.2) is:

$$\mathbf{s}(\mu,t) = \begin{bmatrix} \theta_x(\mu,t) \\ \theta_y(\mu,t) \\ \theta_z(\mu,t) \\ v_x(\mu,t) \\ v_y(\mu,t) \\ v_z(\mu,t) \end{bmatrix} =$$

$$= \begin{bmatrix} \frac{\mu^5 s_{51}}{l^5} + \frac{s_{01}(l-\mu)^5}{l^5} + \frac{5\mu s_{11}(l-\mu)^4}{l^5} + \frac{5\mu^4 s_{41}(l-\mu)}{l^5} + \frac{10\mu^2 s_{21}(l-\mu)^3}{l^5} + \frac{10\mu^3 s_{31}(l-\mu)^2}{l^5} \\ \frac{\mu^5 s_{52}}{l^5} + \frac{s_{02}(l-\mu)^5}{l^5} + \frac{5\mu s_{12}(l-\mu)^4}{l^5} + \frac{5\mu^4 s_{42}(l-\mu)}{l^5} + \frac{10\mu^2 s_{22}(l-\mu)^3}{l^5} + \frac{10\mu^3 s_{32}(l-\mu)^2}{l^5} \\ \frac{\mu^5 s_{53}}{l^5} + \frac{s_{03}(l-\mu)^5}{l^5} + \frac{5\mu s_{13}(l-\mu)^4}{l^5} + \frac{5\mu^4 s_{43}(l-\mu)}{l^5} + \frac{10\mu^2 s_{23}(l-\mu)^3}{l^5} + \frac{10\mu^3 s_{33}(l-\mu)^2}{l^5} \\ \frac{\mu^5 s_{54}}{l^5} + \frac{s_{04}(l-\mu)^5}{l^5} + \frac{5\mu s_{14}(l-\mu)^4}{l^5} + \frac{5\mu^4 s_{44}(l-\mu)}{l^5} + \frac{10\mu^2 s_{24}(l-\mu)^3}{l^5} + \frac{10\mu^3 s_{34}(l-\mu)^2}{l^5} \\ \frac{\mu^5 s_{55}}{l^5} + \frac{s_{05}(l-\mu)^5}{l^5} + \frac{5\mu s_{15}(l-\mu)^4}{l^5} + \frac{5\mu^4 s_{45}(l-\mu)}{l^5} + \frac{10\mu^2 s_{25}(l-\mu)^3}{l^5} + \frac{10\mu^3 s_{35}(l-\mu)^2}{l^5} \\ \frac{\mu^5 s_{56}}{l^5} + \frac{s_{06}(l-\mu)^5}{l^5} + \frac{5\mu s_{16}(l-\mu)^4}{l^5} + \frac{5\mu^4 s_{46}(l-\mu)}{l^5} + \frac{10\mu^2 s_{26}(l-\mu)^3}{l^5} + \frac{10\mu^3 s_{36}(l-\mu)^2}{l^5} \end{bmatrix} \tag{3.14}$$

where l is beam length.

In the present application, the flexible beams are deformed by their mutual interaction and by the rigid motion of the whole system. The model can be formalized by defining all the generalized coordinates, which can be gathered in a vector called $\mathbf{q}$. The latter consists of 86 parameters as a whole, remembering that the sliders are massless and can be considered only as kinematic constraints. For each of the two flexible beams there are 43 parameters: 36 of them are the coefficients of the Bézier polynomials that represent the beam deformation, 6 for each components of vector $\mathbf{s}$, and the remaining 7 completely define the pose of the local frame of reference $\{1\}$ with respect to fixed frame $\{0\}$; 7 parameters are justified by the choice of Euler parameters instead of Euler angles. It follows that such parameters are related by the known normalization equation, namely $\phi_n^i = e_0^i + e_1^i + e_2^i + e_3^i - 1 = 0$ with $i = AB$

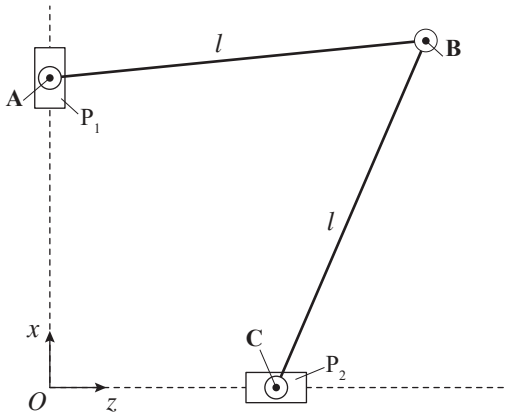

Figure 3.3.: Example of a parallel kinematics machine with 2 degrees of freedom

or BC. According to equations (3.9) and (3.10), both kinetic and potential energies are expressed as the sum of two terms, each of which refers to one of the flexible beams of the system.

By performing symbolic calculations, it results easy to show that the motion equation (3.12) of the parallel mechanism of Figure 3.3 are formed by the following terms:

- $\mathbf{M}$ is the general mass matrix which in turns contains the individual mass matrix of the flexible links, as well as the normalization equations. Particularly, $\mathbf{M}$ is expressed as:

$$\mathbf{M} = \begin{bmatrix} \mathbf{M}^{AB}_{43\times 43} & \mathbf{0}_{43\times 43} \\ \mathbf{0}_{43\times 43} & \mathbf{M}^{BC}_{43\times 43} \end{bmatrix} \tag{3.15}$$

  where the size of $\mathbf{M}$ is 86×86.

- $\mathbf{q}$ is the vector of generalized coordinates of size 86×1, which is composed of the 36 parameters s^{AB}_{ij} with $i = 1 \dots 6$ and $j = 1 \dots 6$, the 7 parameters $x^{AB}_C, y^{AB}_C, z^{AB}_C, e^{AB}_0, e^{AB}_1, e^{AB}_2, e^{AB}_3$ and the other 43 parameters coming from the other link BC.

- the constraint vector $\mathbf{\Phi}$, whose constraint matrix $\mathbf{\Phi}_q$ has been already shown in equation (3.12) and which must satisfy the condition $\mathbf{\Phi} = \mathbf{0}$, is given by the composition of different constraints due to the three revolute joints in points A, B and C, to the behaviour of the flexible links at their extremes and to the actuation of the two sliders. Here it follows the description of each of these contributions:

– $\mathbf{\Phi}_A$ represents the constraint vector of the revolute joint in A with the addition of the actuation of the relative carriage (along the x axis):

$$\mathbf{\Phi}_A = \begin{bmatrix} x - u \\ y \\ z \\ [0\,1\,0]\ \mathbf{R}_{rig,AB} \begin{bmatrix} 1 \\ 0 \\ 0 \end{bmatrix} \\ [0\,1\,0]\ \mathbf{R}_{rig,AB} \begin{bmatrix} 0 \\ 0 \\ 1 \end{bmatrix} \end{bmatrix} \tag{3.16}$$

– $\mathbf{\Phi}_C$ represents the constraint vector of the revolute joint in C, adding also the actuation of the relative carriage (along the z axis):

$$\mathbf{\Phi}_C = \begin{bmatrix} x \\ y \\ z - w \\ [0\,1\,0]\ \mathbf{R}_{rig,BC} \begin{bmatrix} 1 \\ 0 \\ 0 \end{bmatrix} \\ [0\,1\,0]\ \mathbf{R}_{rig,BC} \begin{bmatrix} 0 \\ 0 \\ 1 \end{bmatrix} \end{bmatrix} \tag{3.17}$$

– $\mathbf{\Phi}_{AB}$ represents the constraint vector acting on the link AB, which imposes a null deformation (both rotation and translation) at point A with respect to the reference frame $\{1\}$ and null moment and shear force at the end B of the beam, modeling the flexible link as a beam clamped at one end and free at the other end:

$$\mathbf{\Phi}_{AB} = \begin{bmatrix} \dfrac{d\theta_x^{AB}(0,t)}{d\mu} \\ \dfrac{d\theta_y^{AB}(0,t)}{d\mu} \\ \dfrac{d\theta_z^{AB}(0,t)}{d\mu} \\ \dfrac{dv_x^{AB}(0,t)}{d\mu} \\ \dfrac{dv_y^{AB}(0,t)}{d\mu} \\ \dfrac{dv_z^{AB}(0,t)}{d\mu} \end{bmatrix} \tag{3.18}$$

with $i = 1, \ldots, 6$.

– $\mathbf{\Phi}_{BC}$ defined exactly as $\mathbf{\Phi}_{AB}$, with the only change in the superscript AB with its replacement BC.

– the last constraint $\mathbf{\Phi}_B$ given by the revolute joint in B imposes the three scalar constraint on the position coordinates and the parallelism of local y axes for the two kinematic chains, providing two further equations in terms of orthogonality conditions:

$$\mathbf{\Phi}_B = \begin{bmatrix} \begin{bmatrix} u \\ 0 \\ -w \end{bmatrix} + \mathbf{R}_{rig,AB} \begin{bmatrix} s_x^{AB}(l) \\ s_y^{AB}(l) \\ \|AB\| + s_z^{AB}(l) \end{bmatrix} - \mathbf{R}_{rig,BC} \begin{bmatrix} s_x^{BC}(l) \\ s_y^{BC}(l) \\ \|BC\| + s_z^{BC}(l) \end{bmatrix} \\ [1\ 0\ 0]\ \mathbf{R}_{flex,AB}^T\, \mathbf{R}_{rig,AB}^T\, \mathbf{R}_{rig,BC}\mathbf{R}_{flex,BC} \begin{bmatrix} 0 \\ 1 \\ 0 \end{bmatrix} \\ [0\ 0\ 1]\ \mathbf{R}_{flex,AB}^T\mathbf{R}_{rig,AB}^T\, \mathbf{R}_{rig,BC}\mathbf{R}_{flex,BC} \begin{bmatrix} 0 \\ 1 \\ 0 \end{bmatrix} \end{bmatrix} \tag{3.19}$$

where $\mathbf{R}_{flex,i} = \mathbf{R}_{x,i}\mathbf{R}_{y,i}\mathbf{R}_{z.i}$, with $i = AB$ or BC, is the product of the three small rotations:

$$\mathbf{R}_{x,i} = \begin{bmatrix} 1 & 0 & 0 \\ 0 & \cos(\theta_x^i(l,t)) & -\sin(\theta_x^i(l,t)) \\ 0 & \sin(\theta_x^i(l,t)) & \cos(\theta_x^i(l,t)) \end{bmatrix}$$

$$\mathbf{R}_{y,i} = \begin{bmatrix} \cos(\theta_x^i(l,t)) & 0 & \sin(\theta_x^i(l,t)) \\ 0 & 1 & 0 \\ -\sin(\theta_x^i(l,t)) & 0 & \cos(\theta_x^i(l,t)) \end{bmatrix}$$

$$\mathbf{R}_{z,i} = \begin{bmatrix} \cos(\theta_x^i(l,t)) & -\sin(\theta_x^i(l,t)) & 0 \\ \sin(\theta_x^i(l,t)) & \cos(\theta_x^i(l,t)) & 0 \\ 0 & 0 & 1 \end{bmatrix}$$

  - Vector $\mathbf{\Phi}_n = [\phi_n^{AB} \quad \phi_n^{BC}]^T$ gathers the two normalization equations.

  Finally, vector $\mathbf{\Phi}$ results from the composition of the vectors defined above, namely $\mathbf{\Phi} = [\mathbf{\Phi}_A^T \quad \mathbf{\Phi}_C^T \quad \mathbf{\Phi}_{AB}^T \quad \mathbf{\Phi}_{BC}^T \quad \mathbf{\Phi}_B^T \quad \mathbf{\Phi}_n^T]^T$.

- Vector $\boldsymbol{\lambda}$ in equation (3.12) gathers all the reaction forces originated in the constraints in points A, B and C, and all the unknowns, not necessarily with an interpretable physical meaning, related to the constraints $\mathbf{\Phi}_{AB}$ and $\mathbf{\Phi}_{BC}$.

Further constraints can be used in the study to confine the motion of the manipulator in the horizontal plane xz shown in Figure 3.3, avoiding deformations out of the plane, for instance imposing null values for the coefficients of the polynomials associated to θ_x and θ_z, letting the corresponding vector $\mathbf{s}$ lie on that plane.

3.2. Elasto-dynamic model by using the Principle of Virtual Works.

As stated before, a second approach to model the flexibility of the links of a parallel kinematic robot is the elasto-dynamic model obtained through the formulation of the Principle of the Virtual Works.

Figure 3.4 shows a representation of a generic robot with parallel kinematics, composed by an assembly of rigid and flexible links.

In the following, the axial deformation of the links will be neglected, whereas only the deformation due to bending will be considered.

On the basis of the latter hypotheses, the resulting deformation is always perpendicular to the beam axis; as a consequence, the flexible links can be modeled as rigid

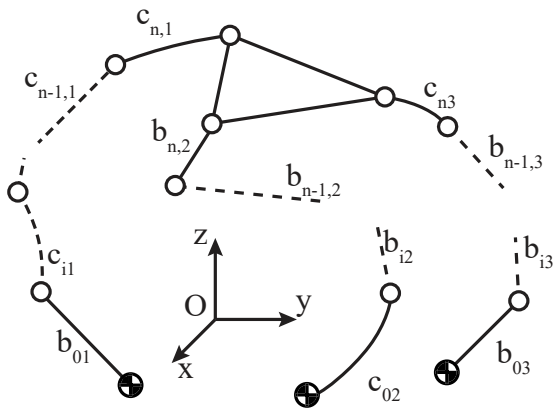

Figure 3.4.: General scheme of a flexible PKM

elements where at their extremes a prismatic joint produces a displacement orthogonal to each flexible link, where such displacement represents the bending deformation. In this way, the deformation of the i^{th} link is expressed as:

$$v(l,t) = \sum_{i=1}^{n} \chi_i(l)\ \eta_i(t) \tag{3.20}$$

where v , composed by the scalar $\chi_i(u)$ that represents the modal form and the scalara $\eta_i(t)$ that represents the harmonic function related to the i^{th} natural frequency, is another degree of freedom of the system, whose value can be computed by solving the dynamic equations since it depends on the stresses the link is subjected to.

Figure 3.5 shows how the stated kinematic equivalence is applied to the system of Figure 3.4. In Figure 3.5 the links coloured in grey are flexible:

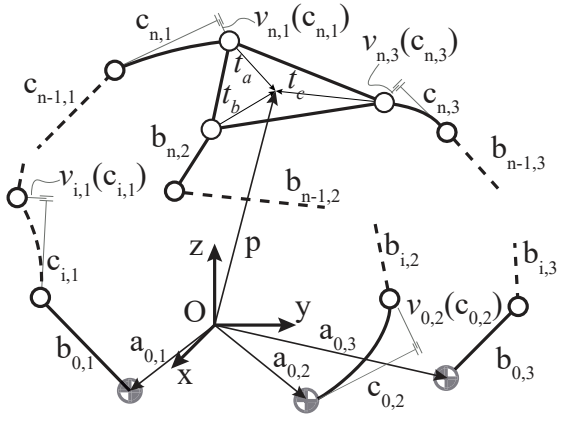

Figure 3.5.: Kinematic equivalence applied to a generic PKM

This approach models the flexible links of a robot as they were rigid. However, the number of joints is increased, which in turn augments the complexity of the whole dynamic system. The payoff of this method is that the accuracy of the solution rises with the number of joints introduced in the modeling phase.

The position equations of the robot showed in Figure 3.5 are derived in the following. Although the system is composed by three links, it that can be modeled by an assembly of m parts, which in turn are divided in n rigid links (indicated with b) and k flexible links (indicate with c):

$$\begin{aligned}
\mathbf{a}_{0,1} + \mathbf{b}_{0,1} + \mathbf{c}_{i,1} + \mathbf{v}_{i1}(c_{i,1}) .. + \mathbf{c}_{n-1,1} + \mathbf{c}_{n,1} + \mathbf{v}_{n,1}(c_{n,1}) + \mathbf{t}_a &= \mathbf{p} \\
\mathbf{a}_{0,2} + \mathbf{c}_{0,2} + \mathbf{v}_{0,2}(c_{0,2}) + \mathbf{b}_{i,2} + ... + \mathbf{b}_{n-1,2} + \mathbf{b}_{n,2} + \mathbf{t}_b &= \mathbf{p} \\
\mathbf{a}_{0,3} + \mathbf{b}_{0,3} + \mathbf{b}_{i,3} + ... + \mathbf{b}_{n-1,3} + \mathbf{c}_{n,3} + \mathbf{v}_{n,3}(c_{n,3}) + \mathbf{t}_c &= \mathbf{p}
\end{aligned}$$

In order to determine the passive joints as a function of the active joints, the following equations can be written:

$$\begin{aligned}
\mathbf{a}_{0,1} + \mathbf{b}_{0,1} + \mathbf{c}_{i,1} + \mathbf{v}_{i1}(c_{i,1}) .. + \mathbf{c}_{n-1,1} + \mathbf{c}_{n,1} + \mathbf{v}_{n,1}(c_{n,1}) + \mathbf{t}_a &= \\
\mathbf{a}_{0,2} + \mathbf{c}_{0,2} + \mathbf{v}_{0,2}(c_{0,2}) + \mathbf{b}_{i,2} + ... + \mathbf{b}_{n-1,2} + \mathbf{b}_{n,2} + \mathbf{t}_b & \\
\mathbf{a}_{0,1} + \mathbf{b}_{0,1} + \mathbf{c}_{i,1} + \mathbf{v}_{i1}(c_{i,1}) .. + \mathbf{c}_{n-1,1} + \mathbf{c}_{n,1} + \mathbf{v}_{n,1}(c_{n,1}) + \mathbf{t}_a &= \\
\mathbf{a}_{0,3} + \mathbf{b}_{0,3} + \mathbf{b}_{i,3} + ... + \mathbf{b}_{n-1,3} + \mathbf{c}_{n,3} + \mathbf{v}_{n,3}(c_{n,3}) + \mathbf{t}_c & \\
\mathbf{a}_{0,2} + \mathbf{c}_{0,2} + \mathbf{v}_{0,2}(c_{0,2}) + \mathbf{b}_{i,2} + ... + \mathbf{b}_{n-1,2} + \mathbf{b}_{n,2} + \mathbf{t}_b &= \\
\mathbf{a}_{0,3} + \mathbf{b}_{0,3} + \mathbf{b}_{i,3} + ... + \mathbf{b}_{n-1,3} + \mathbf{c}_{n,3} + \mathbf{v}_{n,3}(c_{n,3}) + \mathbf{t}_c &
\end{aligned}$$

The latter represents a system of nonlinear equations, which depends on the deformation parameters. Therefore, the kinematic problem presented before becomes:

$$\mathbf{f}(\mathbf{q}, \theta, \mathbf{v}) = 0 \tag{3.21}$$

From equation (3.21), it is possible to obtain the velocity problem as its time derivative:

$$\mathbf{J}_x \dot{\mathbf{p}} = \mathbf{J}_q \dot{\mathbf{q}} + \mathbf{J}_v \dot{\mathbf{v}}$$

When matrix $\mathbf{J}_x$ has full rank, it can be inverted to solve the linear system to compute the Cartesian velocity $\dot{\mathbf{p}}$ as a function of a known $\dot{\mathbf{q}}$. In the same way, matrix $\mathbf{J}_q$ must have full rank in order to compute the actuated joint velocities as a function of known Cartesian velocities. Finally, the acceleration problem can be obtained as the

time derivative of the velocity problem:

$$\mathbf{J}_x\ddot{\mathbf{p}} = \dot{\mathbf{J}}_q\dot{\mathbf{q}} + \mathbf{J}_q\ddot{\mathbf{q}} + \dot{\mathbf{J}}_v\dot{\mathbf{v}} + \mathbf{J}_v\ddot{\mathbf{v}} - \dot{\mathbf{J}}_x\dot{\mathbf{p}}$$

Here, similar considerations can be made regarding matrices $\mathbf{J}_x$ and $\mathbf{J}_q$ in order to solve the direct and inverse acceleration problem and respectively compute $\ddot{\mathbf{p}}$ and $\ddot{\mathbf{q}}$ as a function of known vector $\ddot{\mathbf{v}}$. Apart from $\mathbf{J}_v$, matrices $\mathbf{J}_x$ and $\mathbf{J}_q$ both depend on passive joint velocities.

3.2.1. Dynamic model

In this section, the dynamic equations of motion will be computed by means of the Principle of Virtual Works and the D'Alambert principle, as also done in [47, 48]. According to this method, a generic rigid link is subjected both to inertia forces and inertia moments which, by means of the D'Alambert principle, are considered external actions.

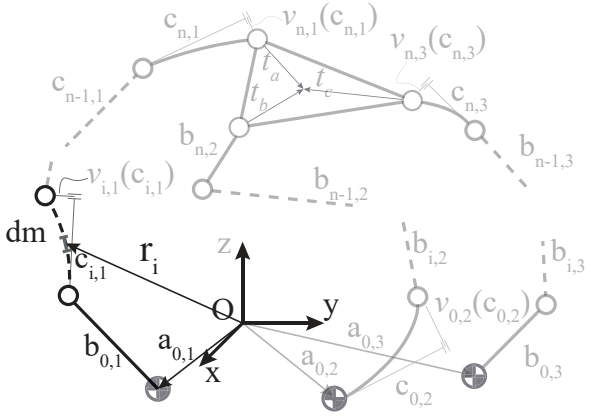

Figure 3.6.: Dynamics behaviour of a generic PKM

Therefore, by considering with $c_{i,1}$ the i^{th} flexible link on the first leg, taken as a reference, the displacement of its generic segment located at the distance u from one end is obtained by following the kinematics of the leg from the fixed frame adding the rigid displacement of the link itself plus its lateral deformation $v_{i,1}(u)$. Thus, the generic position of this element with respect to frame $\{0\}$ is expressed as:

$$\mathbf{r}_i = \mathbf{a}_{0,1} + \mathbf{b}_{0,1} + \mathbf{u} + \mathbf{v}_{i,1}(u)$$

The acceleration of the element can be easily obtained by deriving the latter expression twice as a function of time.

According to D'Alembert principle, the computed acceleration represents the external force which is responsible for the beam deformation. The virtual displacements associated to this force can be computed as:

$$\delta \mathbf{r}_i = \frac{\partial(\mathbf{a}_0 + \mathbf{u} + \mathbf{v}_{a_i}(u))}{\partial(\mathbf{q}, \boldsymbol{\theta}, \mathbf{v})} \begin{bmatrix} \delta\mathbf{q} \\ \delta\boldsymbol{\theta} \\ \delta\mathbf{v} \end{bmatrix} \tag{3.22}$$

In the same way, the virtual angular displacements of the i^{th} passive joint can be easily derived from (3.21) as follows:

$$\begin{aligned} &\delta\theta_i = -\left[\mathbf{A}^{-1}\mathbf{B}\right]_{(i,:)} \delta\mathbf{q}_t, \\ &\text{with} \quad \mathbf{A} = \frac{\partial \mathbf{f}}{\partial \boldsymbol{\theta}} \quad \text{and} \quad \mathbf{B} = \frac{\partial \mathbf{f}}{\partial \mathbf{q}_t}. \end{aligned} \tag{3.23}$$

The virtual displacement δv_i in (3.22) can be easily calculated from the following expression:

$$\delta v_i(u_i) = \sum_{j=1}^{n} \chi_{i,j}(u_i)\delta\eta_{i,j}(t) = \mathbf{X}_i \delta\boldsymbol{\eta}_i, \tag{3.24}$$

The equation (3.22) can written in a compact form:

$$\delta \mathbf{r}_i = \mathbf{E}_{2x2(n+1)} \delta\mathbf{q}_t \tag{3.25}$$

Apart from the inertial forces due to rigid motion, the i^{th} section is subjected to elastic forces, damping forces and inertial deformation as showed by the following expression:

$$\mathbf{F}_{u_i} = \mathbf{F}_{u_i}^{in} + \mathbf{F}_{K_i} + \mathbf{F}_{D_i}, \tag{3.26}$$

where the three forces are:

$$\begin{aligned} \mathbf{F}_{u_i}^{in} &= -\rho A \ddot{\mathbf{r}}_i \mathrm{d}u_i \\ \mathbf{F}_{K_i} &= -EI_z \mathbf{R} \begin{bmatrix} 0 \\ \dfrac{\partial^4 v_i(u_i,t)}{\partial u_i^4} \end{bmatrix} \mathrm{d}u_i \\ \mathbf{F}_{D_i} &= -CI_z \mathbf{R} \begin{bmatrix} 0 \\ \dfrac{\partial^4 \dot{v}_i(u_i,t)}{\partial u_i^4} \end{bmatrix} \mathrm{d}u_i \end{aligned} . \tag{3.27}$$

where $\mathbf{R}$ represents the rotation matrix that give the direction of the middle axis of the link in the undeformed state. It is now possible to compute the virtual work produced by the force $\mathbf{F}_{u_i}$ for a cross sectional element and evaluate its overall effect on the

flexible links by means of the following integral:

$$L_{c_i} = \int_0^c \delta \mathbf{q}_t{}^T \mathbf{E}^T \mathbf{F}_{u_i} du = \delta \mathbf{q}_t{}^T \int_0^c \mathbf{E}^T \mathbf{F}_{u_i} du \qquad i = 1 : k \tag{3.28}$$

For the sake of completeness, it is worthy to compute the work of the forces acting on by the rigid beam; by considering the term $\mathbf{b}_{0,i}$, and assuming that its centre of gravity is placed in the middle, it is:

$$\mathbf{r}_{G_{b_i}} = \mathbf{R}_{\alpha_i} \begin{bmatrix} a \\ 0 \end{bmatrix} + \mathbf{R}_{q_i} \begin{bmatrix} \frac{b}{2} \\ 0 \end{bmatrix};$$

which, in turn, corresponds to the acceleration:

$$\ddot{\mathbf{r}}_{G_{b_i}} = \mathbf{S}_{\ddot{q}_i} \mathbf{R}_{q_i} \begin{bmatrix} \frac{b}{2} \\ 0 \end{bmatrix} - \dot{q}_i^2 \mathbf{R}_{q_i} \begin{bmatrix} \frac{b}{2} \\ 0 \end{bmatrix}$$

Then, the virtual work is:

$$\delta \mathbf{r}_{G_{b_i}} = \mathbf{S}\mathbf{R}_{q_i} \begin{bmatrix} \frac{b}{2} \\ 0 \end{bmatrix} \delta q_i = \mathbf{D}_{(2\times 1)} \delta q_i$$

Said $\mathbf{F}_i^{in}$ and $\mathbf{M}_i^{in}$ respectively the force of inertia and the torque of inertia, the work of the rigid system is equal to:

$$W = \sum_{j=1}^{m} \sum_{i=1}^{n} \left(\delta q_i \mathbf{D}^T \mathbf{F}_{b_i} + \delta q_i M_{b_i}^{in} \right) \tag{3.29}$$

Finally, it results that:

$$W = \sum_{j=1}^{m} \sum_{i=1}^{n,k} \left(\delta q_i \mathbf{D}^T \mathbf{F}_{b_i} + \delta q_i M_{b_i}^{in} + L_{c_i} \right) + \delta \mathbf{q}^T \boldsymbol{\tau} = 0. \tag{3.30}$$

where i refers to the links of the robot.

3.2.2. An application of the model

In order to compare this approach with the one discussed in Section 3.1, an elastic-dynamic model has been developed for the planar mechanism analyzed in Section 3.1.1.

The prismatic joints of Figure 3.6 are actuated, whereas the passive joints are indicated with θ_1, θ_2; finally, the deformations are indicated as v_1, v_2. Particularly, the latter have been modeled by the following equation, meaning that the first two modes have been chosen:

$$v(u,t) = \sum_{i=1}^{2} \chi_i(u)\, \eta_i(t) \tag{3.31}$$

The position of the end-effector B can be computed as:

$$\mathbf{r} = \mathbf{p}_u + \mathbf{R}_1 \begin{bmatrix} l \\ v_1(l) \\ 0 \end{bmatrix} \tag{3.32}$$

$$\mathbf{r} = \mathbf{p}_v + \mathbf{R}_2 \begin{bmatrix} l \\ v_2(l) \\ 0 \end{bmatrix} \tag{3.33}$$

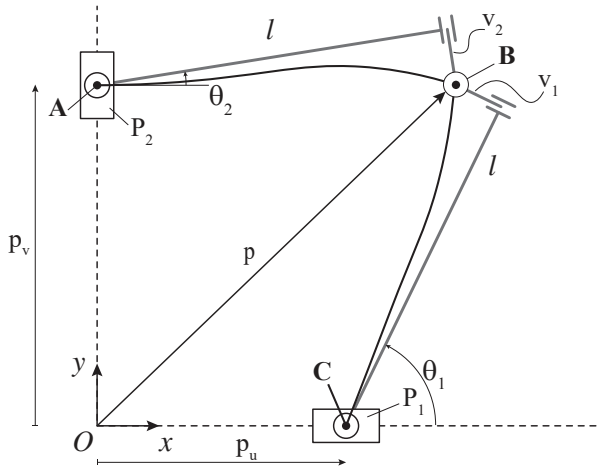

Figure 3.7.: Interpretation of the flexible links as a Revolute-Prismatic sequence of joints

The positions obtained following the two branches must coincide:

$$\mathbf{p}_u + \mathbf{R}_1 \begin{bmatrix} l \\ v_1(l) \\ 0 \end{bmatrix} = \mathbf{p}_v + \mathbf{R}_2 \begin{bmatrix} l \\ v_2(l) \\ 0 \end{bmatrix} \tag{3.34}$$

By decomposing equation (3.34) in the x and y direction, it results:

$$p_u + l\ \cos(\theta_1) - l\ \cos(\theta_2) - v_1\ \sin(\theta_1) + v_2\ \sin(\theta_2) \tag{3.35}$$
$$v_1\ \cos(\theta_1) - p_v - v_2\ \cos(\theta_2) + l\ \sin(\theta_1) - l\ \sin(\theta_2) \tag{3.36}$$

By solving equation (3.36), the passive joints can be obtained as a function of the active joints and the active coordinates. Particularly, two solutions have been computed both for θ_1 both θ_2, whose compact expressions are:

$$\theta_1 = f(p_u, p_v, v_1, v_2) \tag{3.37}$$
$$\theta_2 = f(p_u, p_v, v_1, v_2) \tag{3.38}$$

The velocity problem is obtain as the derivative of (3.33):

$$\mathbf{J}_x\dot{\mathbf{x}} = \mathbf{J}_q\dot{\mathbf{q}} + \mathbf{J}_v\dot{\mathbf{v}} \tag{3.39}$$

where:

$$\mathbf{J}_x = \begin{pmatrix} l\ \cos(\theta_1) - X_1\, c_{01}\ \sin(\theta_1) & l\ \sin(\theta_1) + X_1\, c_{01}\ \cos(\theta_1) \\ l\ \cos(\theta_2) - X_2\, c_{02}\ \sin(\theta_2) & l\ \sin(\theta_2) + X_2\, c_{02}\ \cos(\theta_2) \end{pmatrix}$$
$$\mathbf{J}_q = \begin{pmatrix} l\ \cos(\theta_1) - X_1\, c_{01}\ \sin(\theta_1) & 0 \\ 0 & l\ \sin(\theta_2) + X_2\, c_{02}\ \cos(\theta_2) \end{pmatrix}$$
$$\mathbf{J}_v = \begin{pmatrix} X_1\, c_{01} & 0 \\ 0 & X_2\, c_{02} \end{pmatrix}$$

The derivative of equation (3.39) leads to the acceleration problem. The equations of motion of beam CB are then finally computed as shown in figure 3.8.

Particularly, $\mathbf{r}_i$ is the position of the infinitesimal beam element dm, whereas its speed is $\dot{\mathbf{r}}_i$ and its acceleration $\ddot{\mathbf{r}}_i$:

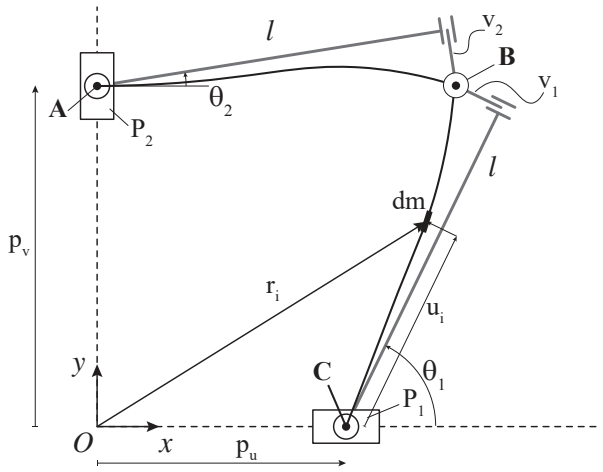

Figure 3.8.: Position of a generic cross section for a flexible link

$$\mathbf{r}_i = \begin{bmatrix} p_u \\ 0 \\ 0 \end{bmatrix} + \mathbf{R}_1 \begin{bmatrix} u_i \\ v_i \\ 0 \end{bmatrix}$$

$$\dot{\mathbf{r}}_i = \begin{bmatrix} \dot{p}_u \\ 0 \\ 0 \end{bmatrix} + \mathbf{S}_1\mathbf{R}_1 \begin{bmatrix} u_i \\ v_i \\ 0 \end{bmatrix} + \mathbf{R}_1 \begin{bmatrix} 0 \\ \dot{v}_i \\ 0 \end{bmatrix}$$

$$\ddot{\mathbf{r}}_i = \begin{bmatrix} \ddot{p}_u \\ 0 \\ 0 \end{bmatrix} + \dot{\mathbf{S}}_1\mathbf{R}_1 \begin{bmatrix} u_i \\ v_i \\ 0 \end{bmatrix} + \mathbf{S}_1^2\mathbf{R}_1 \begin{bmatrix} u_i \\ v_i \\ 0 \end{bmatrix} + 2\mathbf{S}_1\mathbf{R}_1 \begin{bmatrix} 0 \\ \dot{v}_i \\ 0 \end{bmatrix} + \mathbf{R}_1 \begin{bmatrix} 0 \\ \ddot{v}_i \\ 0 \end{bmatrix}$$

From $\ddot{\mathbf{r}}_i$, the inertial force acting on the element can be calculated by using equation (3.27). As for virtual displacement $\mathbf{r}_i$, it results that:

$$\delta\mathbf{r}_i = \begin{bmatrix} 1 \\ 0 \\ 0 \end{bmatrix} \delta p_u + \mathbf{S}_1\mathbf{R}_1 \begin{bmatrix} u_i \\ v_i \\ 0 \end{bmatrix} \delta\theta_1 + \mathbf{R}_1 \begin{bmatrix} 0 \\ 1 \\ 0 \end{bmatrix} \delta v_1(u_i) \tag{3.40}$$

where $\delta\theta_1$ can be calculated by equation 3.23, where $i = 1$. Then, by considering both the rigid and the flexible contributions, the virtual work of the beam results in:

$$L_{c_i} = \int_0^c \delta\mathbf{r}_i^T \mathbf{F}_{u_i} du \tag{3.41}$$

The same computations can be performed on beam AB; therefore, the total virtual work for the whole mechanism is expressed by:

$$W = \sum_{i=1}^{2} \left(\delta \mathbf{q}^T \boldsymbol{\tau} + L_{c_i} \right). \tag{3.42}$$

3.3. Comparison of the models

The approaches presented above represent two alternative methods to model a robot with flexible links. Since the purpose of this work is to choose the most suitable model for a real-time control, it is necessary to investigate the performance of the proposed solutions. In order to achieve this result, the computation time has been assessed for a given, known trajectory.

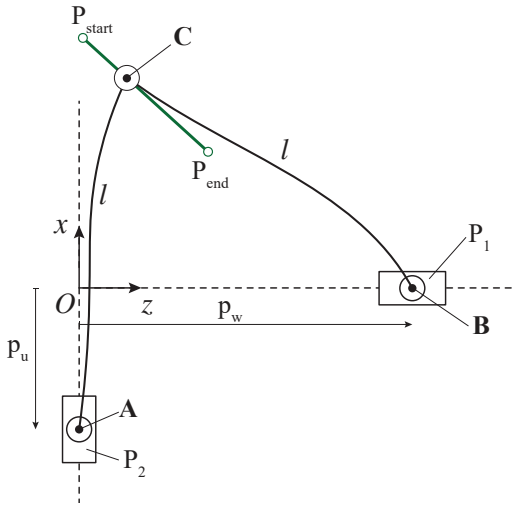

Figure 3.9.: Linear trajectory between two Cartesian points used for testing

Figure 3.9 shows the robot configurations as the end-effector moves according to the planned path. Particularly, the end effector represented by point C will move along a straight line starting from point P_{start} to the final point P_{end}; here, the initial and final conditions are zero-velocity and zero-acceleration.

Figure 3.10 shows the average computation time for the planned path. The measured time has been normalized with respect to the time computed when the robot is modeled by using the Bernastein polynomial. The simulations have been performed on a desktop computer with an Intel Core i7-6700HQ processor with a clockspeed equal to 2.60 [GHz].

The comparative analysis shows that the approach where the deformation of the beam has been modeled with the assumed mode methods has the lowest computation

time. Therefore, it has been chosen in the following to model the robot under study, remembering the need of a light model to be computed with the final aim of a model-based control application.

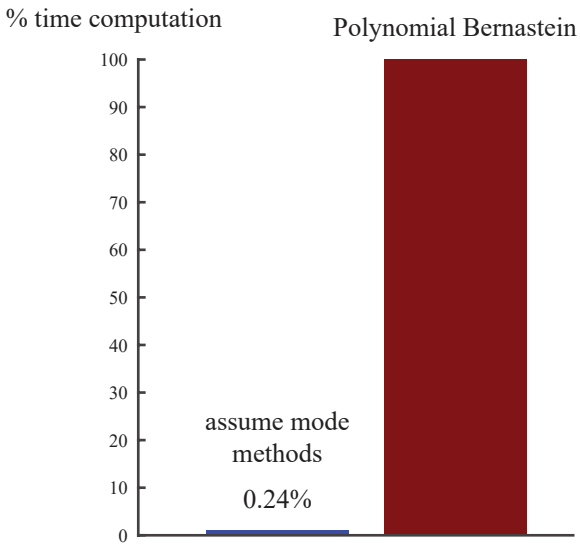

Figure 3.10.: Comparison of computational burden for the two proposed algorithms

Chapter 4.

Elasto-dynamic model of a five-bar linkage

In this chapter an elasto-dynamic model for a closed loop mechanism is presented, namely a five-bar linkage, using a Lagrangian approach with a minimum set of parameters. The deformations are modelled by the Assumed Modes Method. The chapter also depicts how the robot dimensions have been chosen, according to the measuring bench available in the MIR Laboratory of the Polytechnic University of Marche. Eventually, a comparative analysis has been carried out among analytical results and simulations have been performed with a FE model, built by means of a commercial software.

4.1. Kinematic model of a flexible five-bar linkage

The robot object of the study is represented in Figure 4.1. It's easy to demonstrate that it owns two degrees of freedom by means of the well known Gruebler equation:

$$q = 3\, n_{cm} - 2\, c_1 - c_2 = 2$$

where n_{cm} indicates the number of movable bodies that make up the kinematics, with c_1 the kinematic pairs that leave one degree of freedom and with c_2 the kinematic pairs that leave two degrees of freedom. For a five bar mechanism there are four movable bodies and five revolute joints belonging to the class c_1.

For the sake of simplicity, only two out of the four links which compose the mechanism are flexible (the distal links), while the remaining two (proximal) own an extremely rigid cross section with respect to the others. This permits to focus the modelling of the flexible components to only a couple of bodies, and to disregard such aspects for the actuated ones.

Also, the system has been designed considering symmetrical lengths of the links. The origin of the absolute reference frame is located in the centerline between points

A_1 and A_2. The x axis intersects such two points and it is directed towards A_1, while the z axis is perpendicular to the plane of the machine.

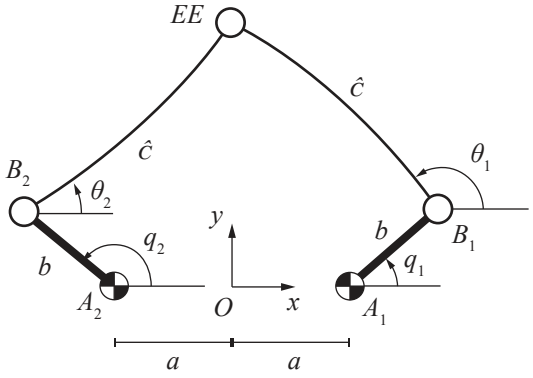

Figure 4.1.: Five bars with flexible links

Since the distal arms deform during motion, the model should take into consideration such effect to predict the position of the robot terminal (here identified by point EE). The modal superposition approach is adopted in this sense, as already described in Section 2.2.1. Therefore, each one of the two flexible links are modeled by means of an equivalent RPR joint topology. It means that, starting from a reference rigid model in which each distal link is connected at its extremes by means of two revolute joints, it can be introduced a virtual body that slides laterally at the distal extreme of the link along its transverse direction by means of a virtual prismatic joint P. The concept is clearly shown in Figure 4.2. In such scheme, the two revolute joints R represent the connection interfaces with the other members of the kinematic chain.

Consequently, the addition of these two new kinematic pairs implies the introduction of two new degrees of freedom which cannot be imposed during the motion of the system. They result from a dynamic equilibrium which involves also the constitutive equations which connect the forces acting on the system, including the inertia forces, to the displacements undergone by the flexible links, which behave like bending springs. According to this statement, the kinematic scheme of the robot becomes the one already mentioned and shown in Figure 4.2.

By referring to the scheme of Figure 4.2, it is easy to find the position of point EE following the i^{th} kinematic branch, with $i = 1, 2$; in particular, said $\mathbf{p}$ the planar vector from the origin of the fixed frame to point EE, the loop closure equations for each loop $O - EE - B_i - A_i$ provide:

$$\mathbf{p} = \mathbf{a}_i + \mathbf{b}_i + \mathbf{c}_i + \mathbf{v}_i \qquad (i = 1, 2) \ , \tag{4.1}$$

where the i^{th} vectors for $i = 1, 2$ are defined as:

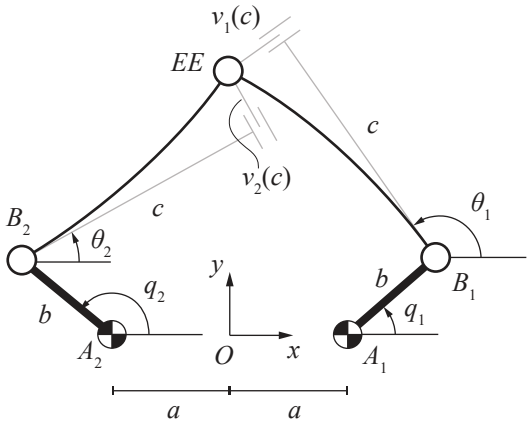

Figure 4.2.: Kinematic modeling of the Pentalateral with flexible arms

$$\mathbf{a}_i = \mathbf{R}_{\alpha_i} \begin{bmatrix} a \\ 0 \end{bmatrix}; \qquad \mathbf{b}_i = \mathbf{R}_{q_i} \begin{bmatrix} b \\ 0 \end{bmatrix}; \qquad \mathbf{c}_i = \mathbf{R}_{\theta_i} \begin{bmatrix} c \\ 0 \end{bmatrix}; \qquad \mathbf{v}_i = \mathbf{R}_{\theta_i} \begin{bmatrix} 0 \\ v_i(c,t) \end{bmatrix}. \tag{4.2}$$

The rotation matrix $\mathbf{R}_\psi$ about the z axis is given in a 2×2 simplified formulation:

$$\mathbf{R}_\psi = \begin{bmatrix} \cos\psi & -\sin\psi \\ \sin\psi & \cos\psi \end{bmatrix} \qquad \text{with } \psi = \alpha_i, q_i, \theta_i,$$

where the angle α_i provides the direction and orientation of vector $\mathbf{s}_i$. In the present work $\alpha_1 = 0$ and $\alpha_2 = \pi$.

Finally $v_i(c,t)$ identifies the value of the deformation at the end of the i^{th} flexible link, which represents the translation of the passive prismatic joint added to describe its lateral flexibility.

The *Direct Kinematic Problem* (DKP) consists of finding the Cartesian position of the end-effector of the robot as a function of the rotations of the actuated revolute joints. Such position is described by the vector indicated with $\mathbf{p}$, which identifies the position of EE with respect to the origin O of the fixed frame shown in Figure in 4.2.

Vector $\mathbf{p}$ can be obtained once the value of the actuated joints q_i are assigned and the lateral deformations v_i are assigned, considered known from static or dynamic analyses for both the i^{th} flexible links. This equation is also a function of the passive joints θ_i, which must be obtained as a function of the active joints. The DKP is then formalized as:

$$\mathbf{f}\left(\mathbf{q}, \boldsymbol{\theta}, \mathbf{v}\right) = \mathbf{0}, \tag{4.3}$$

which can be mad explicit as follows:

$$\begin{cases} c\left(\cos\theta_1 - \cos\theta_2\right) - v_1(c,t)\sin\theta_1 + v_2(c,t)\sin\theta_2 = b\left(\cos q_2 - \cos q_1\right) - 2a \\ c\left(\sin\theta_1 - \sin\theta_2\right) + v_1(c,t)\cos\theta_1 - v_2(c,t)\cos\theta_2 = b\left(\sin q_2 - \sin q_1\right) \end{cases}, \tag{4.4}$$

The inverse kinematics problem (IKP) consists of finding the position of the actuated joints once a Cartesian position of the end-effector EE is assigned, i.e. when vector $\mathbf{p}$ is known.

Since the deformation of the flexible links does not depend on the position but on the loading conditions, at this stage it is considered that the deformation is known in order to find the values of the actuated joints. Referring to the i^{th} branch of the manipulator shown in 4.2, equation (4.1) can be rearranged by isolating the actuated joint variables, still unknown at the moment:

$$\begin{cases} b\cos\left(q_i\right) = x_{EE} - a\cos\left(\alpha_i\right) - c\cos\left(\theta_i\right) + v_i\sin\left(\theta_i\right) \\ b\sin\left(q_i\right) = y_{EE} - c\sin\left(\theta_i\right) - v_i\cos\left(\theta_i\right) \end{cases}. \tag{4.5}$$

By squaring and adding the two scalar equations, it is possible to get rid of the actuated joint variables, thus obtaining an expression that is only a function of the passive joint variables θ_i and of the deformation variables $v_i(c,t)$, from here on indicated without brackets to improve the readability of the equations:

$$A\cos(\theta_i) + B\sin(\theta_i) + C = 0, \tag{4.6}$$

with:

$$\begin{aligned} A &= -2\left(x_{EE} - a\cos\alpha_i\right)c - 2y_{EE}v_i \\ B &= 2\left(x_{EE} - a\cos\alpha_i\right)v_i - 2y_{EE}c \\ C &= \left(x_{EE} - a\cos\alpha_i\right)^2 + y_{EE}^2 + c^2 + v_i^2 - b^2 \end{aligned}$$

Two solutions exist for each passive joint angle θ_i, each of which provides a value for q_i. The algorithm used to solve the equation (4.6) requires a verification of the domain of the existence of the root, which must be satisfied to have real solutions. As expected, four different configurations can be found from the combination of the branches even if only one of them is acceptable once the assembly configuration is known.

4.1.1. Differential Kinematics

The derivative of the loop closure equations (4.1) provides:

$$\dot{\mathbf{p}} = \mathbf{S}_{\dot{q}_i}\mathbf{R}_{q_i}\begin{bmatrix} b \\ 0 \end{bmatrix} + \mathbf{S}_{\dot{\theta}_i}\mathbf{R}_{\theta_i}\begin{bmatrix} c \\ v_i \end{bmatrix} + \mathbf{R}_{\theta_i}\begin{bmatrix} 0 \\ \dot{v}_i \end{bmatrix} \tag{4.7}$$

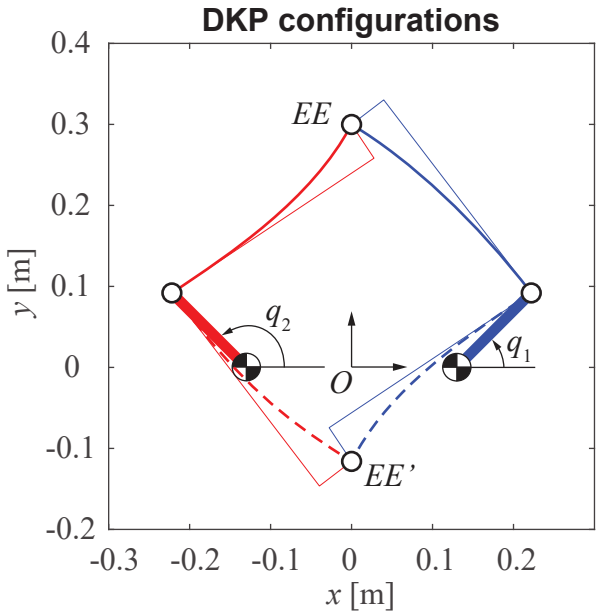

Figure 4.3.

where:

$$\mathbf{S}_{\dot{\psi}} = \mathbf{S}\dot{\psi} \qquad \text{with } \mathbf{S} = \begin{bmatrix} 0 & -1 \\ 1 & 0 \end{bmatrix} \text{ and } \dot{\psi} = \dot{q}_i, \dot{\theta}_i, \text{ for } i = 1, 2.$$

The relationship between $\dot{\mathbf{p}} = [\dot{x}_{EE}, \dot{y}_{EE}]^T$ and the vector $\dot{\mathbf{q}} = [\dot{q}_1, \dot{q}_2]^T$ of the actuated joint velocities can be obtained when the value of the deformations of the members $\mathbf{v} = [v_1, v_2]^T$ is known, and the strain rate vector $\dot{\mathbf{v}} = [\dot{v}_1, \dot{v}_2]^T$ is known. The velocities of the passive joints $\dot{\theta}_i$ can be removed from the equation (4.7) by means of the following scalar product:

$$\begin{bmatrix} c & v_i \end{bmatrix} \mathbf{R}_{\theta_i}^T \dot{\mathbf{p}} = \begin{bmatrix} c & v_i \end{bmatrix} \mathbf{R}_{\theta_i}^T \mathbf{S}_{\dot{q}_i} \mathbf{R}_{q_i} \begin{bmatrix} b \\ 0 \end{bmatrix} + \begin{bmatrix} c & v_i \end{bmatrix} \begin{bmatrix} 0 \\ \dot{v}_i \end{bmatrix} . \tag{4.8}$$

The two equations obtained from (4.8) can be rewritten in a more compact form as:

$$\mathbf{J}_x \dot{\mathbf{p}} = \mathbf{J}_q \dot{\mathbf{q}} + \mathbf{J}_v \dot{\mathbf{v}}, \tag{4.9}$$

where the matrices are:

$$\mathbf{J}_x = \begin{bmatrix} c\cos\theta_1 - v_1\sin\theta_1 & c\sin\theta_1 + v_1\cos\theta_1 \\ c\cos\theta_2 - v_2\sin\theta_2 & c\sin\theta_2 + v_2\cos\theta_2 \end{bmatrix}, \tag{4.10}$$

$$\mathbf{J}_q = b\begin{bmatrix} c\sin(\theta_1 - q_1) + v_1\cos(\theta_1 - q_1) & 0 \\ 0 & c\sin(\theta_2 - q_2) + v_2\cos(\theta_2 - q_2) \end{bmatrix}, \tag{4.11}$$

$$\mathbf{J}_v = \begin{bmatrix} v_1 & 0 \\ 0 & v_2 \end{bmatrix}. \tag{4.12}$$

When matrix $\mathbf{J}_x$ has full rank, it can be inverted to solve the linear system of Cartesian velocity $\dot{\mathbf{p}}$ for a given $\dot{\mathbf{q}}$. On the contrary, a full rank for $\mathbf{J}_q$ is required when the joint velocity vector is searched for a given Cartesian velocity of point EE.

The conditioning of both $\mathbf{J}_x$ and $\mathbf{J}_q$ will be discussed later. The velocity of the passive joints $\dot{\theta}_i$ can be found directly from (4.7) by means of the following scalar product:

$$\begin{bmatrix} b & 0 \end{bmatrix}\mathbf{R}_{q_i}^T\dot{\mathbf{p}} = \begin{bmatrix} b & 0 \end{bmatrix}\mathbf{R}_{q_i}^T\mathbf{S}\mathbf{R}_{\theta_i}\begin{bmatrix} c \\ v_i \end{bmatrix}\dot{\theta}_i + \begin{bmatrix} b & 0 \end{bmatrix}\mathbf{R}_{q_i}^T\mathbf{R}_{\theta_i}\begin{bmatrix} 0 \\ \dot{v}_i \end{bmatrix}, \tag{4.13}$$

which provides a solution for $\dot{\theta}_i$ when its coefficient differs from zero; the problem owns a singularity when the three points A_i, B_i, and EE are aligned, namely when:

$$\tan(q_i - \theta_i) \neq \frac{v_i}{c}. \tag{4.14}$$

When the vector $\dot{\mathbf{q}}$ of the actuated joints is assigned, instead of the Cartesian velocity $\dot{\mathbf{p}}$, the value of the passive joints can be found from (4.13) by means of (4.9).

The acceleration problem is obtained by means of a time derivative of (4.9):

$$\mathbf{J}_x\ddot{\mathbf{p}} = \dot{\mathbf{J}}_q\dot{\mathbf{q}} + \mathbf{J}_q\ddot{\mathbf{q}} + \dot{\mathbf{J}}_v\dot{\mathbf{v}} + \mathbf{J}_v\ddot{\mathbf{v}} - \dot{\mathbf{J}}_x\dot{\mathbf{p}}, \tag{4.15}$$

where analogous considerations can be made regarding matrices $\mathbf{J}_x$ and $\mathbf{J}_q$ in order to be able to solve the direct and inverse problem of acceleration between $\ddot{\mathbf{p}}$ and $\ddot{\mathbf{q}}$, once given $\ddot{\mathbf{v}}$, with clear meaning of all terms.

In the end, it can be noted that $\dot{\mathbf{J}}_v$, whose expression can be easily derived from (4.12), does not depend on the speed of the passive joints obtained from (4.13), unlike matrices $\dot{\mathbf{J}}_x$ and $\dot{\mathbf{J}}_q$.

4.1.2. Number of Independent Variables

The choice of a number n of modes in (2.24) determines the number of independent variables involved in both the kinematics and dynamics models of the manipulator. A

more detailed notation is used from here on to better investigate the dynamics of the flexible five-bar linkage.

Said $v_i(u_i, t)$ the transverse displacement of the generic cross section placed at the distance u_i from the clamped end of the i^{th} flexible beam, as shown in Figure 4.2, a number of $2(n+1)$ independent variables can be defined:

$$\mathbf{q}_t(t) = \begin{bmatrix} \mathbf{q}(t) \\ \boldsymbol{\eta}_1(t) \\ \boldsymbol{\eta}_2(t) \end{bmatrix}_{2(n+1)\times 1} \tag{4.16}$$

where $\boldsymbol{\eta}_i = [\eta_{i,1}, \ldots, \eta_{i,n}]^T$. The space eigenfunctions χ follow the same notation, providing for each j^{th} mode of the i^{th} link the expression $\chi_{i,j}$.

4.2. Elasto-Dynamic model

The same approach proposed in Section 3.2.1 is here exploited to model the elasto-dynamics of the flexible five-bar linkage, whose kinematics has been already investigated in the previous section.

Inertial forces, acting on the center of mass of each link, and moments can be considered as external contributions according to the D'Alembert Principle. Before taking into account the flexibility of its distal links, a five-bar linkage made of only rigid links can be considered in order to find the most influential contribution due to inertial terms:

$$\begin{array}{ll} \mathbf{F}_{b_i}^{in} = -m_b \ddot{\mathbf{r}}_{G_{b_i}} & \mathbf{F}_{c}^{in} = -m_c \ddot{\mathbf{r}}_{G_{c_i}} \\ M_{b_i}^{in} = -I_b \ddot{q}_i & M_{c}^{in} = -I_c \ddot{\theta}_i \end{array} \quad \text{with} \quad i = 1, 2, \tag{4.17}$$

where where $\ddot{\mathbf{r}}_{G_{b_i}}$ and $\ddot{\mathbf{r}}_{G_{c_i}}$ represent the acceleration vectors of the center of mass of links b and c respectively. Inertial contributions tend to expressions (4.17) when a null deformation v_i is hypothesized for the two links of length c. The position vector of the center of mass of all moving bodies is required in (4.17) to find acceleration expressions. The position G_{b_i} of the centers of mass of the rigid links can be easily found. On the contrary, if flexibility is taken into account, as shown in Figure 4.4, a local study on each cross section of the flexible links must be addressed. The position of points G_{b_i} and of a generic cross section of infinitesimal mass $dm = \rho A \mathrm{d}u$, can be found with respect to the fixed frame $\{O; x, y\}$ as:

$$\mathbf{r}_{G_{b_i}} = \mathbf{R}_{\alpha_i} \begin{bmatrix} a \\ 0 \end{bmatrix} + \mathbf{R}_{q_i} \begin{bmatrix} \frac{b}{2} \\ 0 \end{bmatrix}; \qquad \mathbf{r}_i = \mathbf{R}_{\alpha_i} \begin{bmatrix} a \\ 0 \end{bmatrix} + \mathbf{R}_{q_i} \begin{bmatrix} b \\ 0 \end{bmatrix} + \mathbf{R}_{\theta_i} \begin{bmatrix} u_i \\ v_i(u_i) \end{bmatrix} \tag{4.18}$$

A time derivative of both the expressions in (4.18) and a further derivative provide the required velocities and accelerations:

$$\begin{array}{l} \dot{\mathbf{r}}_{G_{b_i}} = \mathbf{S}_{\dot{q}_i} \mathbf{R}_{q_i} \begin{bmatrix} \frac{b}{2} \\ 0 \end{bmatrix} \\ \dot{\mathbf{r}}_i = \mathbf{S}_{\dot{q}_i} \mathbf{R}_{q_i} \begin{bmatrix} b \\ 0 \end{bmatrix} + \mathbf{S}_{\dot{\theta}_i} \mathbf{R}_{\theta_i} \begin{bmatrix} u_i \\ v_i(u_i) \end{bmatrix} + \mathbf{R}_{\theta_i} \begin{bmatrix} 0 \\ \dot{v}_i(u_i) \end{bmatrix} \end{array}, \tag{4.19}$$

and

$$\ddot{\mathbf{r}}_{G_{b_i}} = \mathbf{S}_{\ddot{q}_i}\mathbf{R}_{q_i}\begin{bmatrix}\frac{b}{2}\\0\end{bmatrix} - \dot{q}_i^2\mathbf{R}_{q_i}\begin{bmatrix}\frac{b}{2}\\0\end{bmatrix}$$

$$\ddot{\mathbf{r}}_i = \mathbf{S}_{\ddot{q}_i}\mathbf{R}_{q_i}\begin{bmatrix}b\\0\end{bmatrix} - \dot{q}_i^2\mathbf{R}_{q_i}\begin{bmatrix}b\\0\end{bmatrix} + \mathbf{S}_{\ddot{\theta}_i}\mathbf{R}_{\theta_i}\begin{bmatrix}u_i\\v_i(u_i)\end{bmatrix} - \dot{\theta}_i^2\mathbf{R}_{\theta_i}\begin{bmatrix}u_i\\v_i(u_i)\end{bmatrix} + \\ +2\mathbf{S}_{\dot{\theta}_i}\mathbf{R}_{\theta_i}\begin{bmatrix}0\\\dot{v}_i(u_i)\end{bmatrix} + \mathbf{R}_{\theta_i}\begin{bmatrix}0\\\ddot{v}_i(u_i)\end{bmatrix} \quad . \tag{4.20}$$

The force $\mathbf{F}_{u_i}$ in Figure 4.4 applied to the cross section located by means of its coordinates u_i, v_i with respect to the local frame $\{B_i; u, v\}$ on each flexible link gathers inertial, elastic and damping force contributions.

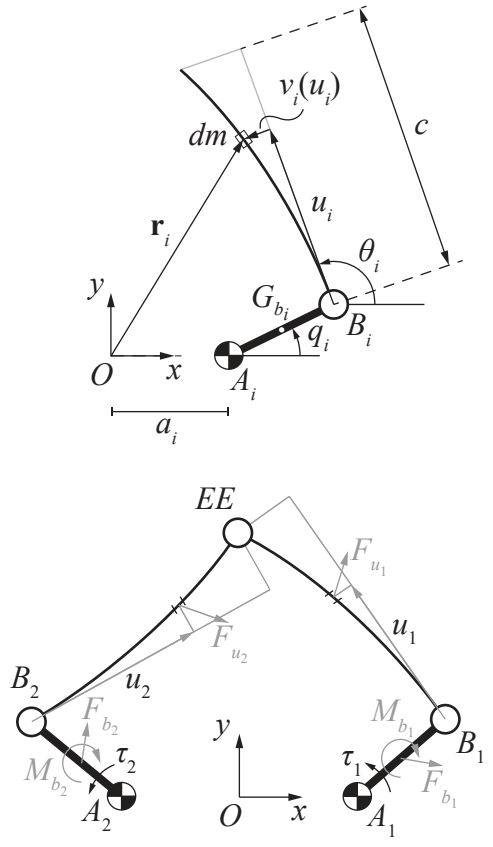

Figure 4.4.: Cross section and position and dynamic loads.

It is given by:

$$\mathbf{F}_{u_i} = \mathbf{F}_{u_i}^{in} + \mathbf{F}_{K_i} + \mathbf{F}_{D_i}, \tag{4.21}$$

The expression of the forces on the right of (4.21) depends on the model proposed in (2.37), after a few arrangements of the partial differential equation due to the integration of the flexible link in a closed kinematic chain. In fact, model (2.37) changes accordingly:

$$-EI_z \frac{\partial^4 v_i\left(u_i,t\right)}{\partial u_i^4} - CI_z \frac{\partial^4 \dot{v}_i\left(u_i,t\right)}{\partial u_i^4} = \rho A \frac{\mathbf{v}_i^T(u_i,t)}{||\mathbf{v}_i||} \ddot{\mathbf{r}}_i \tag{4.22}$$

where the term on the right assumes the following explicit form:

$$\frac{\mathbf{v}_i^T(u_i,t)}{||\mathbf{v}_i||} \ddot{\mathbf{r}}_i = b\ddot{q}_i \cos\left(q_i-\theta_i\right) - b\dot{q}_i^2 \sin\left(q_i-\theta_i\right) + u_i\ddot{\theta}_i - v_i\left(u_i\right)\dot{\theta}_i^2 + \ddot{v}_i\left(u_i\right). \tag{4.23}$$

It follows that the three forces in (4.21) are now completely defined, assuming the expressions shown in (3.27), where the rotation matrix involved in the study is $\mathbf{R} = \mathbf{R}_{\theta_i}$. The virtual work of such forces can be worked out once the virtual displacement of their application points is obtained:

$$\delta\mathbf{r}_i = \mathbf{S}\mathbf{R}_{q_i} \begin{bmatrix} b \\ 0 \end{bmatrix} \delta q_i + \mathbf{S}\mathbf{R}_{\theta_i} \begin{bmatrix} u_i \\ v_i(u_i) \end{bmatrix} \delta\theta_i + \mathbf{R}_{\theta_i} \begin{bmatrix} 0 \\ 1 \end{bmatrix} \delta v_i(u_i) \tag{4.24}$$

The virtual angular displacement of the i^{th} passive joint can be easily derived from (4.3) by using the same approach proposed in (3.23), here recalled for the sake of clarity:

$$\delta\theta_i = -\left[\mathbf{A}^{-1}\mathbf{B}\right]_{(i,:)} \delta\mathbf{q}_t \tag{4.25}$$

The inversion of matrix $\mathbf{A}$ is possible only when (4.14) is satisfied, whose relative configuration is quite far from normal operating conditions. The virtual displacement δv_i in (4.24) can be easily found from (2.24):

$$\delta v_i(u_i) = \sum_{j=1}^{n} \chi_{i,j}(u_i)\delta\eta_{i,j}(t) = \mathbf{X}_i\delta\boldsymbol{\eta}_i, \tag{4.26}$$

with $\mathbf{X}_i = \begin{bmatrix}\chi_{i,1} & \chi_{i,2} & \dots & \chi_{i,n}\end{bmatrix}$. Finally, the required expression for $\delta\mathbf{r}_{G_{b_i}}$ and $\delta\mathbf{r}_i$ can be found as a function of the independent virtual displacements:

$$\delta \mathbf{r}_{G_{b_i}} = \mathbf{S}\mathbf{R}_{q_i} \begin{bmatrix} \frac{b}{2} \\ 0 \end{bmatrix} \delta q_i = \mathbf{D}_{(2\times 1)} \delta q_i$$

$$\begin{aligned} \delta \mathbf{r}_i &= \mathbf{S}\mathbf{R}_{q_i} \begin{bmatrix} b \\ 0 \end{bmatrix} \delta q_i - \mathbf{S}\mathbf{R}_{\theta_i} \begin{bmatrix} u_i \\ v_i(u_i) \end{bmatrix} \left[\mathbf{A}^{-1}\mathbf{B}\right]_{(i,:)} \delta \mathbf{q}_t + \mathbf{R}_{\theta_i} \begin{bmatrix} 0 \\ 1 \end{bmatrix} \mathbf{X}_i \delta \boldsymbol{\eta}_i \\ &= \mathbf{E}_{(2\times 2(n+1))} \delta \mathbf{q}_t \end{aligned} \tag{4.27}$$

It is now possible to evaluate the virtual work produced by the force $\mathbf{F}_{u_i}$ in (4.21) for a cross sectional element, and to evaluate its overall effect on the flexible links by means of the following line integral:

$$L_{c_i} = \int_0^c \delta \mathbf{q}_t{}^T \mathbf{E}^T \mathbf{F}_{u_i} = \delta \mathbf{q}_t{}^T \int_0^c \mathbf{E}^T \mathbf{F}_{u_i} \qquad i = 1, 2 \tag{4.28}$$

The total virtual work of the flexible five-bar manipulator is therefore:

$$W = \sum_{i=1}^{2} \left(\delta q_i \mathbf{D}^T \mathbf{F}_{b_i} + \delta q_i M_{b_i}^{in} + L_{c_i} \right) + \delta \mathbf{q}^T \boldsymbol{\tau} = 0. \tag{4.29}$$

The arbitrariness of $\delta \mathbf{q}_t^T$ in equation (4.29), after few arrangements, allows to obtain a system of ordinary differential equations, written only in terms of independent variables:

$$\mathbf{M}\ddot{\mathbf{q}}_t = \boldsymbol{\Gamma}(\mathbf{q}_t, \dot{\mathbf{q}}_t, t) \tag{4.30}$$

where $\mathbf{M}$ is a $2(n+1) \times 2(n+1)$ mass matrix and $\boldsymbol{\Gamma}(\mathbf{q}_t, \dot{\mathbf{q}}_t, t)$ is a vector collecting all dynamic terms that do not depend on accelerations. Desired model accuracy or time integration issues guide the choice of a proper number n for the modes in (4.30).

4.3. Simulation plant design

Having now a general elasto-dynamic model for a five-bars, in order to carry out simulations on a real case study, it is necessary to define both physical and geometric parameters. Their values have been designed to ensure compatibility between the equipment available at the MIR Lab (Laboratory of Mechatronics and Industrial Robotics of the Polytechnic University of Marche, in Italy) and the performance that is required to the parallel robot.

In particular, a testbench has been conceived according to Figure 4.5, where two se-

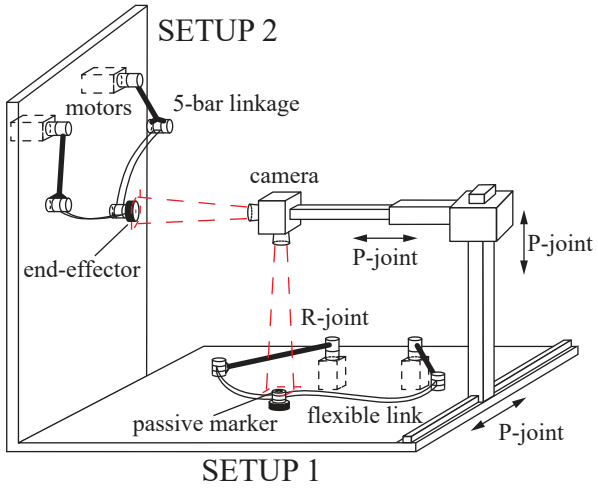

Figure 4.5.: Testbench concept.

tups can be arranged in order to test the manipulator in different operating conditions. More details will be given in the following. However, the main idea is to use a fast camera as an exteroceptive sensor pointing towards the end-effector of the five-bar linkage in order to acquire its position at a high frame rate. The resulting data can be used to identify several parameters, from kinematics to dynamics, so that model-based controls can be implemented to improve the dynamic performance of the robot. Therefore, the features of the camera have an impact on the maximum oscillation frequencies that can be observed for the position of the robot end-effector during its motion, affecting its mechanical design.

The hardware mentioned above is made up of the following items:

- Basler a504k camera $1280\,[\text{px}] \times 1024\,[\text{px}]$ with $500\,[\text{fps}]$ and $12\,[\mu\text{m}] \times 12\,[\mu\text{m}]$ pixel size, used as exteroceptive sensor for pose estimation;
- NI PXIe-1435 Camera Link Frame Grabber;
- Lens with focal length f of $50\,[\text{mm}]$.

As already mentioned, this equipment imposes constraints on the size of flexible members and their geometry, in fact considering that the camera has a frame rate of $500\,[\text{fps}]$, the maximum frequency that can be detected according to the Nyquist–Shannon sampling theorem is:

$$f_c = \frac{f_s}{2}$$

where f_s is the frequency of the signal, whereas f_c is the sampling rate. From this equation, it is evident that to detect the first 3 oscillation modes of the flexible links, their geometries must comply with the constraints imposed by the available equipment. In particular, the dimension of the links has been chosen so that at least 3 natural frequencies fall under 125 [Hz], knowing that:

- the maximum sampling rate of 500 [Hz] for the camera is purely theoretic and reachable under certain strict conditions;
- the software dedicated at grabbing and processing images needs time by itself to be executed.

The constraint imposed above can be guaranteed by choosing three parameters: the material, namely the Young's modulus E and the density ρ, their cross section A, and the length of the beam. Using steel bodies with $E = 2e^{11}$ [Pa], the length and the section remain to be set.

The length of the flexible links influences both the frequencies of the links themselves and the manipulator workspace (for this purpose further details can be found in [49]). In particular, by choosing a length of the flexible links equal to $c = 0.3$ [m] and rigid links with a length $b = 0.13$ [m], the resulting workspace is free of singularities within the boundaries of the chosen assembly mode. Moreover, a significant manipulability is also available in the robot workspace, as shown in the following section.

With the aim of obtaining the aforementioned properties in terms of vibrations, a rectangular section with $w_c \times h_c = 0.5$ [mm] $\times 10$ [mm] is chosen. A summary of the geometric properties is shown in Table 4.1, which shows the section of the rigid links also.

Table 4.1.: Geometric dimension of links.

length [mm]	section [mm] × [mm]	mass [kg]	inertia [kg·m^2]
$a = 130$	–	–	–
$b = 130$	$w_b \times h_b = 25 \times 25$	$m_b = 0.634$	$I_b = 9.25 \cdot 10^{-4}$
$c = 300$	$w_c \times h_c = 0.5 \times 10$	$m_c = 0.012$	$I_c = 8.77 \cdot 10^{-5}$

The two parameters E and C needed to compute the elasto-dynamic model proposed in this work can be identified by means of experimental tests in order to find their actual value. In this work, if not specified, it is chosen $C = 0.003$ [MPa s], for E a value has already been assigned.

Besides the acquisition frequency of the camera, another important parameter is the position resolution that the camera is able to detect. As a matter of fact, the oscillation

that the end-effector of the manipulator could be subject to, must be detectable by the camera with sufficient accuracy. The choice of a more performing system both in terms of frame rate and resolution would allow to investigate a higher frequency content with a more precise measurement of the end-effector position. Accordingly, the vertical arrangement of the camera with respect to the robot must be defined in order to improve the measurement quality. The testbench presented in Figure 4.5 meets all these needs.

More in detail, two setups can be arranged:

- in "SETUP 1" it is assumed that the flexible links are not influenced by their weight because in that direction the stiffness of the beams is enough to avoid a motion out of the horizontal plane. Therefore, in this case the deformation of the flexible links is caused only by the actuation torques and by the inertia acting on the horizontal plane.
- in "SETUP 2", on the contrary, gravity affects the behaviour of the system, and therefore it cannot be neglected. Such setup shows similarities with the typical architecture of a Delta Robot: the ABB Flexpicker is an example of fast and slender parallel robot used in many industrial applications where high dynamic loads are involved and must be taken into account. The proposed setup allows to simplify the study in a smaller domain without losing generality.

Finally, another important aspect is the influence of the distance of the camera with respect to the end-effector, whose acquisition area in Figure 4.5 is shown in red. In particular, by positioning the camera in a plane placed at a distance of 245 mm from the end-effector, an effective frame of $75.24\text{mm} \times 60.16$ mm can be obtained. In such conditions the camera performs with a position resolution of about 0.059 mm in its acquisition plane.

4.4. Compliance Analysis

Limiting the study to only the first mode for each flexible link, which is the mode with greater amplitude, a compliance analysis can be performed.

By looking at the formulation obtained previously for the differential kinematics, some new arrangements can be done:

$$\begin{aligned} &\dot{\boldsymbol{\eta}} = \mathbf{X}^{-1}\mathbf{J}_v^{-1}\left(\mathbf{J}_x\dot{\mathbf{p}} - \mathbf{J}_q\dot{\mathbf{q}}\right) \\ &\text{with } \mathbf{X}(c) = \begin{bmatrix} \chi_{1,1}(c) & 0 \\ 0 & \chi_{2,1}(c) \end{bmatrix} \text{ and } \dot{\boldsymbol{\eta}} = \begin{bmatrix} \dot{\eta}_{1,1} \\ \dot{\eta}_{2,1} \end{bmatrix}, \end{aligned} \tag{4.31}$$

where the actuated joint variables are kept separate from the harmonic function η. Applying a set of deformation velocities with unit norm $\dot{\boldsymbol{\eta}}^T\dot{\boldsymbol{\eta}} = 1$, it follows that:

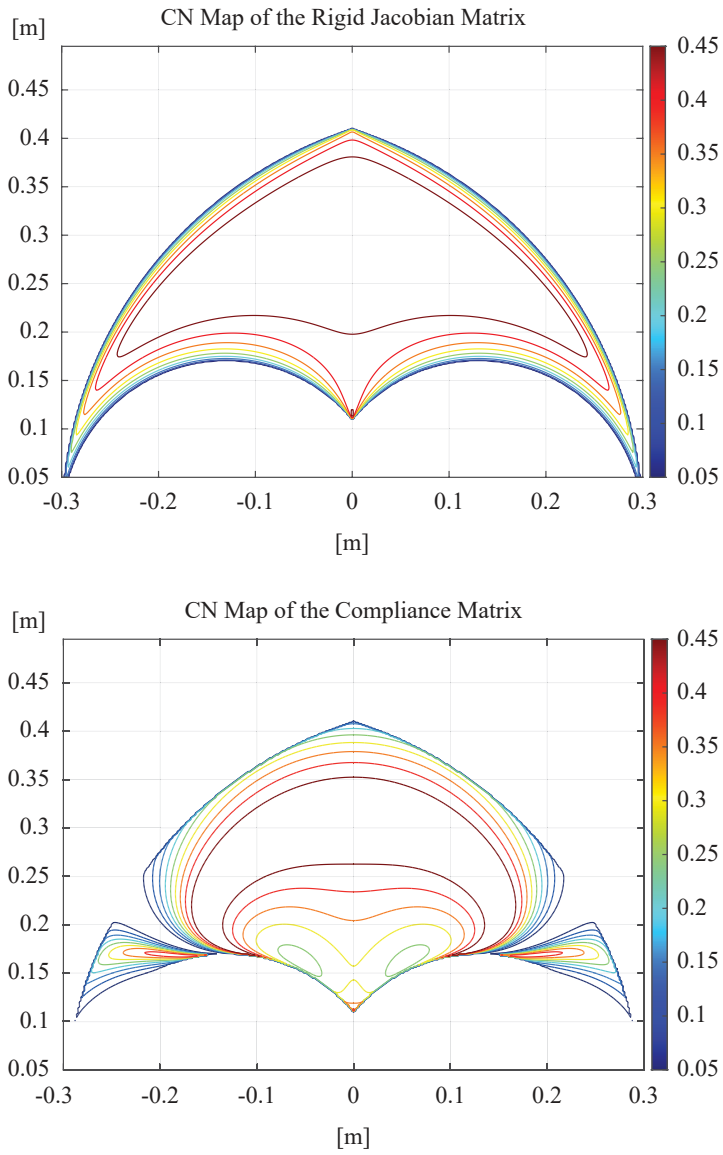

Figure 4.6.: Map of the condition number based on the Frobenius norm for a rigid and a flexible five-bar linkage.

$$\left(\dot{\mathbf{p}} - \mathbf{J}_x^{-1}\mathbf{J}_q\dot{\mathbf{q}}\right)^T \mathbf{J}_x^T\mathbf{J}_v^{-T}\mathbf{X}^{-T}\mathbf{X}^{-1}\mathbf{J}_v^{-1}\mathbf{J}_x \left(\dot{\mathbf{p}} - \mathbf{J}_x^{-1}\mathbf{J}_q\dot{\mathbf{q}}\right), \tag{4.32}$$

Studying the matrix $\mathbf{C} = \mathbf{J}_x^T\mathbf{J}_v^{-T}\mathbf{X}^{-T}\mathbf{X}^{-1}\mathbf{J}_v^{-1}\mathbf{J}_x$ throughout the manipulator workspace, the areas of maximum and minimum compliance are highlighted. Null values are assigned to $\eta_{1,1}$ and $\eta_{2,1}$ in order to evaluate the effect of deformation ve-

locities of links in an undeformed configuration. Figure 4.6 shows two colour maps that represent the trend of the condition number based on the Frobenius norm for both a rigid and a flexible five-bar linkage.

As expected, the highest stiffness is associated with configurations of the manipulator where the arms are perpendicular to each other. This phenomenon is related to the fact that the bending deformation that would occur on one link would translate as an axial load on the other link. In the boundaries of the workspace the condition number tends to zero since the flexible links have a relative orientation far from the most rigid perpendicular configuration.

4.5. Results

In this section, some results about the effectiveness of the proposed elasto-dynamic model in terms of both accuracy and computational efficiency are presented. The flexible links are based on the first 4 modal forms, discussing whether they are sufficient or not for the objective set only at the end of the study.

In particular, using a circular trajectory, the model presented has been compared with a Finite Element model. Subsequently, the model presented has been analyzed in detail in order to show how it behaves and how many modal shapes are needed. Finally, a comparison of all the models used in this work will conclude the investigation in order to identify the most performing model from the computational point of view.

4.5.1. Comparing the elasto-dynamic model with finite element model

In order to analyze the elasto-dynamic model of the robot, the law given to the torques of the actuated joints has been derived from the inverse dynamics of a five-bar linkage with all rigid links. The applied torques are calculated to make the end-effector complete a circular trajectory within its workspace in the time of 1 second.

The chosen trajectory has a radius $r = 0.025\ [m]$ and it is accomplished by starting and arriving with null speed and acceleration. To model the curvilinear abscissa of the circular path a Bézier polynomial of fifth order has been used. This polynomial has six coefficients that can be found applying an equal number of conditions.

More specifically, the following conditions have been set:

- initial displacement $p_i = [0.05 \quad 0.25]^t$
- final displacement $p_f = [0 \quad 0.25]^t$
- initial and final speed equal zero
- initial and final acceleration equal zero

By means of a Bézier polynomial the time law has been found. The torque laws follow a preliminary study about the inverse kinematics of the robot with rigid links followed by the use of its inverse dynamic model. Such laws are shown in Figure 4.7.

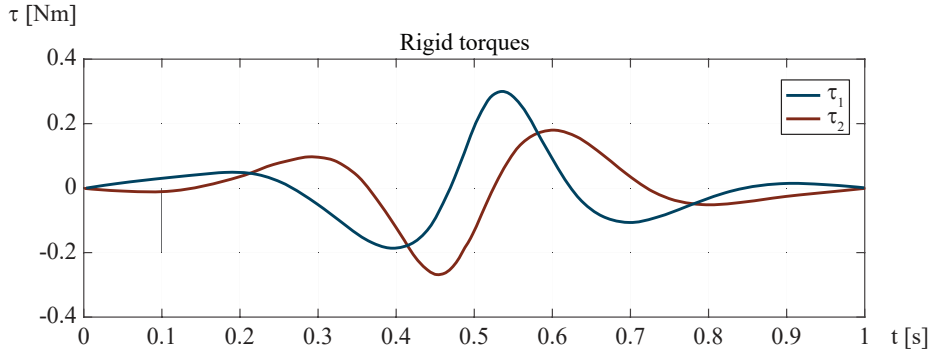

Figure 4.7.: Torque values obtained from a Cartesian circular motion of five-bar linkage with rigid links

These torques have been applied both to the analytical model presented above and to a model created in a FE simulation environment. The latter has been realized by modeling the flexible links of the robot with 16 elements for each beam. The number of elements has been chosen so that the code remains light from the computational point of view but with the necessary precision to be able to describe the phenomenon under study.

In particular, by dividing each link into sixteen elements based the "beam 189" Ansys element, which is suitable to analyse slender structures, 33 nodes have been obtained, each one having 6 degrees of freedom. By applying the constraints in order to obtain a planar model, the resulting model incorporates 64 vibration modes for each beam. The trend of the end-effector position over time for both models along the x and y Cartesian directions is shown in Figures 4.8.

Due to the small deformation values, it is not possible to clearly see the difference between the elasto dynamic model and the FE model taken as reference for its verification. Therefore, the error made by the robot end-effector with respect to the planned trajectory is shown along the x and y directions, as shown in Figure 4.9.

The overall error of the end-effector in carrying out the planned trajectory has been calculated as:

$$e_{tot} = \sqrt{e_x^2 + e_y^2} \tag{4.33}$$

and its trend is shown in Figure 4.10.

From the trend of the error calculated as the difference between the position of the end-effector of the rigid robot and of the flexible robot, it is easy to verify that the order

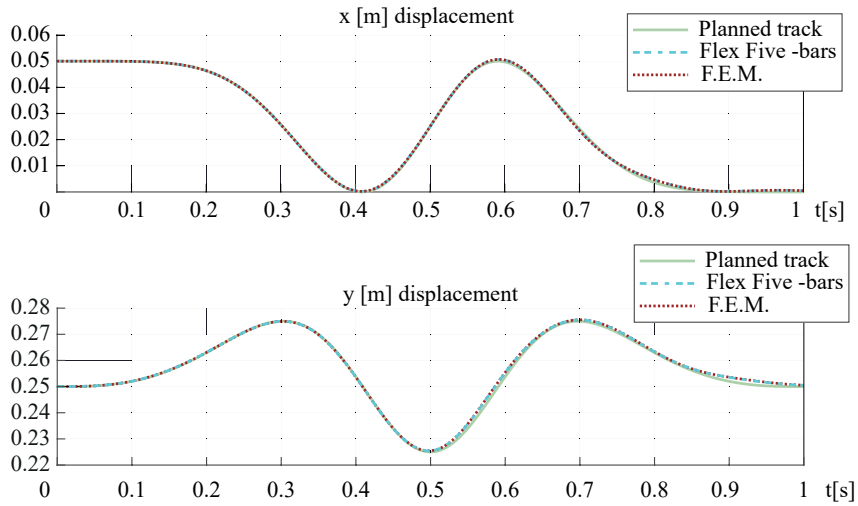

Figure 4.8.: Comparison of the Cartesian trajectories obtained for a FE model and the proposed elasto-dynamic model

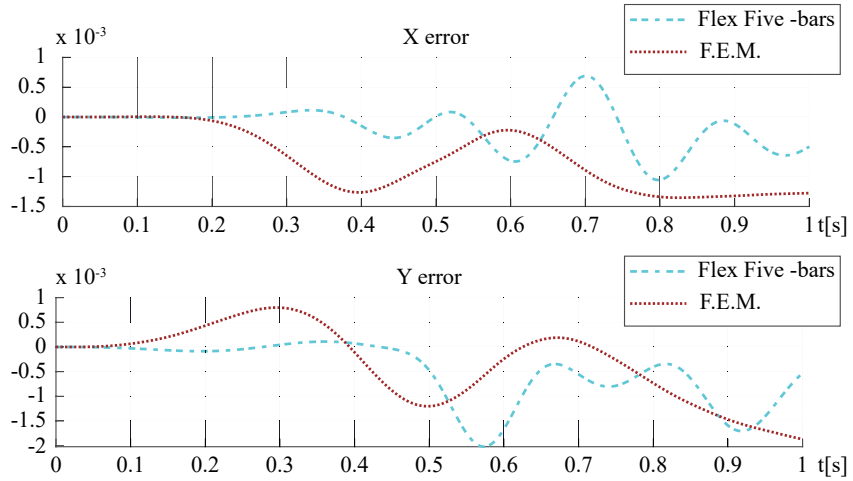

Figure 4.9.: Comparison between the Cartesian trajectories for a FE model and the proposed elasto-dynamic model in terms of Cartesian errors

of magnitude of the error of the two models is the same. The trends, as expected, have some similarities but do not coincide. By suitably varying the damping coefficient C, the behaviour of the elasto-dynamic model can be adjusted to be closer to the FE model or more importantly to the data obtained from the end-effector trajectory of a real robot.

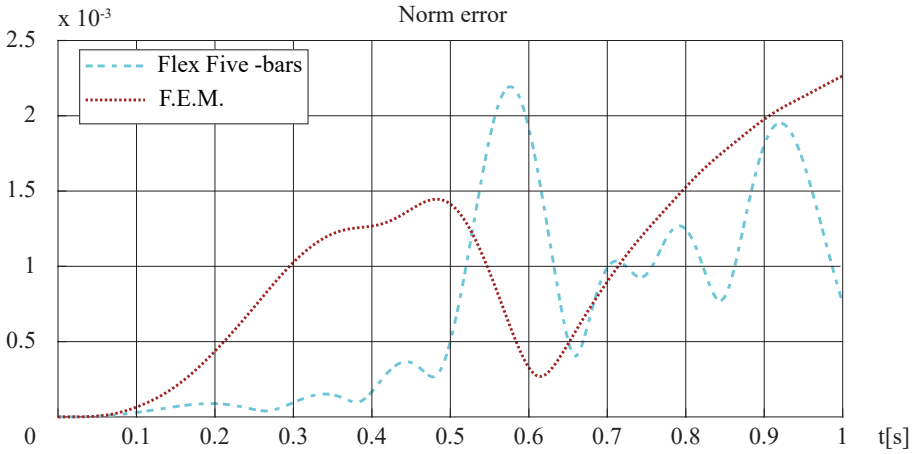

Figure 4.10.: Norm of the overall Cartesian error obtained by a comparison between the FE model and the elastodynamic model

4.5.2. Analysis of the elastodynamic model

To better understand the proposed model, an analysis of its behavior with respect to a given circular trajectory has been addressed. In this simulation the damping coefficient is set as $C = 0$ [MPa s] in order to have no damping effect on the flexible members. The simulation presented in this case consists of two parts:

- Part I - the robot completes a turn of a circular trajectory in one second, with zero speed and acceleration conditions at the beginning and end of the trajectory.
- Part II - no torques are applied to the robot (zero torques to the actuators); this part of the simulation has a duration of eleven seconds, here the only effect is related to the deformation energy accumulated during the motion and to the residual speed and acceleration from the circular motion.

Therefore, the total simulation lasts 12 seconds. This value has been chosen in order to be able to clearly see the oscillations that the robot makes after executing the imposed trajectory. The simulation shows that, following the motion imposed by the motors and calculated through the inverse dynamics of the rigid robot, the end-effector moves in a position in the neighborhood of the planned one and with a certain non-null speed and acceleration.

The presence of the a certain residual energy at the end of the motion is due to the flexibility of the links, which store a part of the work done by the actuators under the form of elastic displacements. Being the motion not controlled to reach the desired position then, the system returns such deformation as oscillations which affect the positioning precision.

Figure 4.11 shows the trend of the couples as a function of time:

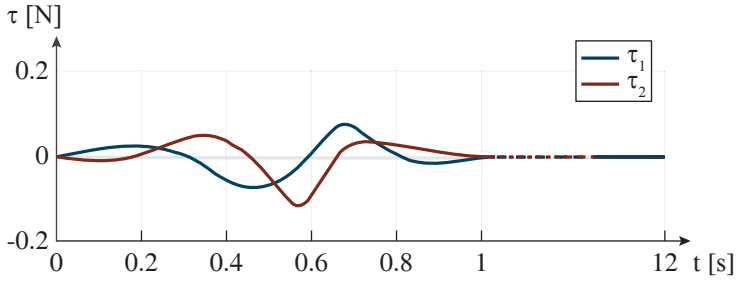

Figure 4.11.: Torques obtained by the rigid model of a five-bar linkage in following a circular path

To analyse the behavior of the flexible links, since these are modeled with the Assumed Modes Method, a study of the trends of the coefficients δ_i is proposed since the information on the amplitude of the oscillations of the various modes can be better appreciated. To this end, the vibration modes of links 1 and 2 are shown in Figure 4.12.

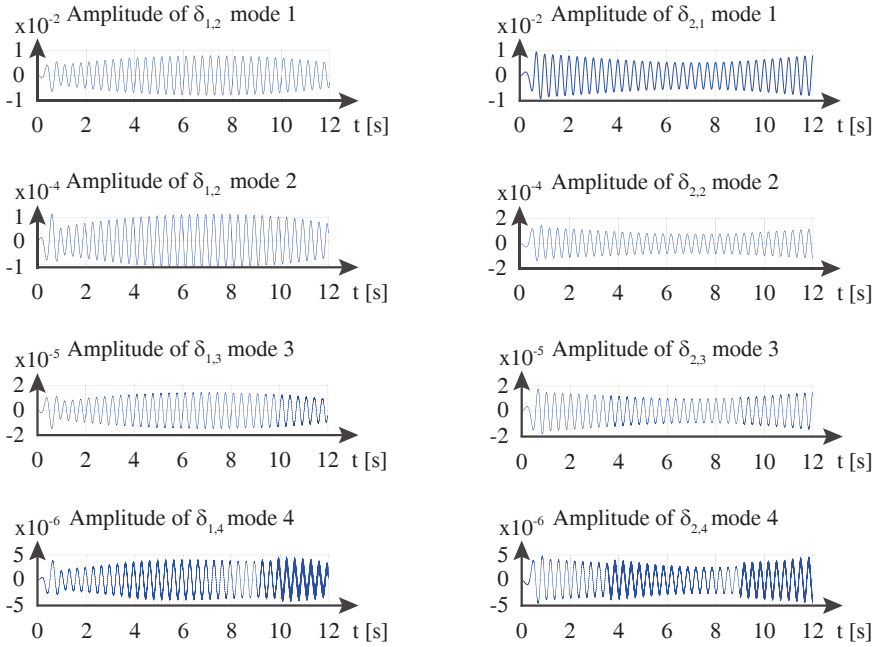

Figure 4.12.: Amplitude of the coefficients of the modal shapes without damping

From Figure 4.12 it can be noted that, in the first part of the simulation, the trend of the amplitude of the coefficients is influenced by the imposed torques. Furthermore, it can be seen that the amplitude of the coefficients of the even modes are out of phase by $180°$ with respect to the odd modes. As expected, it can be also noticed that the

deformation amplitude of the modes decreases the more the mode is at high frequency.

In the second part, there is an evident transfer of energy between the amplitude coefficients of links 1 and 2; in particular, it can be seen that the generic i^{th} mode of link 1 is out of phase by $180°$ with respect to the same mode of link 2. This is due to the absence of damping in this simulation.

With the introduction of damping, with a value of $C = 0.0003$ [MPa s], a trend similar to that already described is obtained, but with fluctuations of smaller amplitude and a period of about 3 seconds; after that, all the coefficients reach a value of zero amplitude, which causes the end-effector of the robot to stop oscillating.

The previous considerations can be summarized by means of Figure 4.13, which shows the trend of the coefficients δ_i for a simulation with damping.

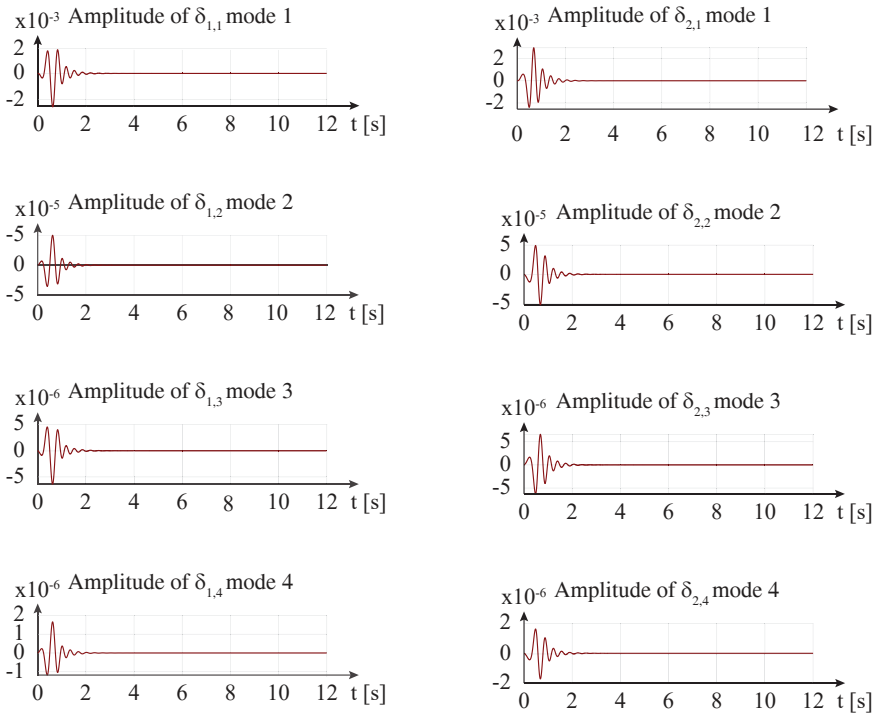

Figure 4.13.: Amplitude coefficients of modal forms with damping

Finally, it is worth noticing that in both simulations the amplitude of the modes are negligible starting from the third one ($\sim 10^{-5}$ and even less for the damped simulation). Therefore, the position of the end-effector EE can be described with sufficient accuracy using the superposition of the first two vibration modes, which are the prevalent ones during dynamic operations.

4.5.3. Algorithm efficiency

After having examined and compared the elasto-dynamic model from the point of view of deformation, the present chapter closes the study by comparing it with all the models used while carrying out this work: a FE model and a model based on the Bézier polynomials.

The comparison is aimed at identifying the calculation time of the model in order to understand if this can in the future be used in a real-time controller.

In order to make this comparison, two types of tests have been carried out, corresponding to two different load conditions.

In the first type of load, a small initial deformation of the flexible links is applied to the models, and the simulation is performed in direct dynamics for a small time interval. The average time obtained from one hundred simulations were performed. The calculator in use is a personal computer having a processor Intel Core i7-6700 HQ with a clockspeed of 2.60 [GHz], which yielded the results in Figure 4.14.

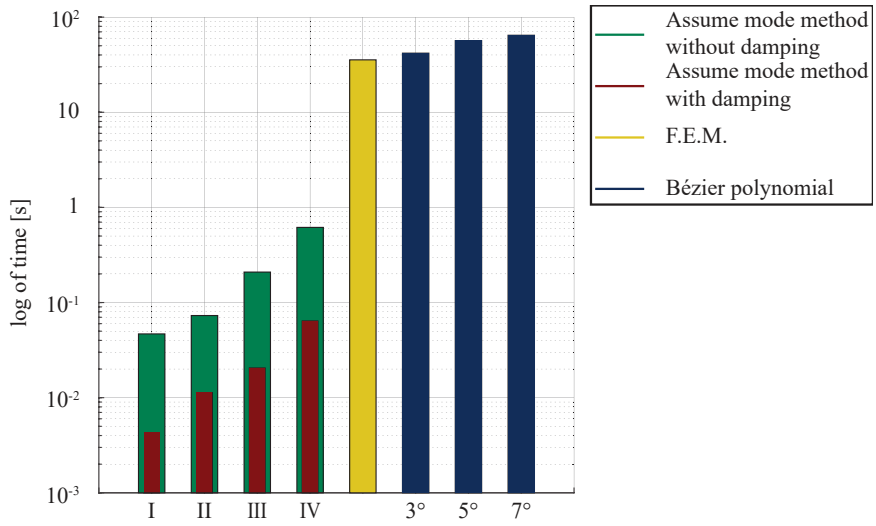

Figure 4.14.: Computation time comparison between several models for a small initial deformation

For the second load case, only the acceleration of gravity has been applied to all the bodies of the model g, without applying any torque to the actuators. Also in this case, a campaign of direct dynamics simulations have been performed for a small interval of time with the same computer. The mean values of the computation times for these simulations lead to the result presented in Figure 4.15.

From the results shown above, it is possible to conclude that the model based on the Assumed Modes is the most performing in terms of computation time.

In particular, the diagrams show that the model with damping can be calculated in 0.01 [s] time and therefore could be applied in real-world scenarios. Naturally more

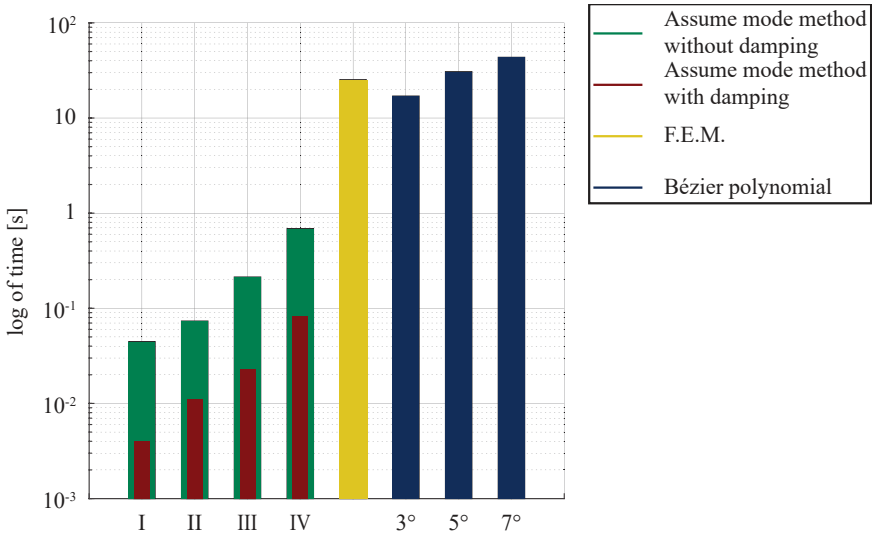

Figure 4.15.: Computation time comparison gravity acceleration applied

investigation on a physical testbench can validate the results obtained in this work or provide suggestions for improving its behavior and computational efficiency.

Chapter 5.

Conclusion and Future works

5.1. Conclusion

In this work an effective approach for the modeling of parallel kinematics robots with flexible links has been presented. In particular, starting from the description and analysis of the methods that describe the dynamics of the deformation of the robot links, different types of elasto-dynamic models for parallel kinematics robots have been developed.

The proposed elasto-dynamic models differ from each other since: in the first, the deformation is described by means of a Bézier polynomial and the equations of motion of the elasto-dynamic model are obtained using the Augmented Formulation of Lagrange, whereas in the second, the deformation is evaluated using the Assumed Mode Method and the dynamics equations are obtained through the Principle of Virtual Works.

Having presented the two models highlighting their intrinsic characteristics, the second approach mentioned above has been chosen. In fact, it has demonstrated the greatest performance in terms of computation time required to be solved. Afterwords, by virtue of this feature, the kinematics and dynamics of a five-bar linkage with flexible links and a kinematic architecture similar to that of a well-known family of industrial robots have been modelled.

The choice of the physical and geometric parameters to be used in the model has been discussed. As a matter of fact, their values are linked to the performance of a testbench conceived to identify the kinematic and dynamic parameters of the robot, based on the equipment available at the MIR Laboratory of the Polytechnic University of Marche. More in detail, the performance of a fast camera belonging to the measuring bench clearly influences the workspace of the robot and the performance which can be detected through the available instrumentation. Therefore, the design of the flexible links followed some guidelines with accordance to the performance of the instrumentation.

Furthermore, the chosen model has been verified by means of a Finite Element model, from which it has emerged that some similarities exist regarding deformations, especially with respect to the order of magnitude. However such study needs further

investigation, so that the behavior is as faithful as possible.

Several studies have been presented on the chosen model in order to show its characteristics and potential; in particular, a link compliance map has been presented in order to identify the areas in which the robot is most compliant inside its workspace, so that a designer can take them into account in the design or planning phase of a task. Finally, the work ends by comparing all the models presented from the computational point of view in order to determine which of them may be considered the best candidate for use in model-based real-time controls.

5.2. Future Works

As mentioned in the introduction, the results of flexible robotics may find application in many fields, from which the industrial sector can benefit most.

This work has been mainly focused on the development of an elasto-dynamic model of parallel kinematics machines and the simulations presented have been conceived to answer the needs of the industrial sector considering applications of industrial robots. In this context, an aspect of considerable interest concerns the improvement that could be obtained through model-based controls of industrial machines with high dynamic performance in trajectory tracking. The hypothesized workbench proposed in the present work has been conceived in order to allow kinematic calibration and identification of dynamic parameters. Such operations have considerable interest in real applications, where mechanical calibration is usually preliminary to the commissioning of a machine. Moreover, the knowledge of an identified elastodynamic model allows to improve the trajectory tracking, extending the range of applicability of a machine to increasingly extreme conditions of use. The results obtained from the computation of the proposed elastodynamic model seem compatible with these purposes.

Therefore, one of the most important activities that can be planned as a future work is the mechanical calibration and identification of the parameters of the proposed elastodynamic model. Hence, a validation of the model is needed by means of a physical testbench in order to fulfill the calibration requirements.

Another aspect of strong interest from an industrial point of view consists in studying how this model behaves following the application of a certain payload, analysing the effect of change in its value. This represents a crucial aspect, since the task of any robot clearly consists in moving a tool installed at the robot end-effector to perform a specific task.

As already mentioned, the elastodynamic model presented in this work is only a preliminary model that takes into account only partially the deformation that a flexible link can exhibit in dynamic conditions. For instance, large displacements can be considered and axial constraints can be introduced to model its physical behaviour.

Finally, the idea of compliant systems in industry is certainly more oriented towards the emerging field of collaborative robotics, where humans and machines share

the same workspace collaborating in a common task. The definition of advanced compliance models could favor the development of more collaborative applications, where the machine can react with compliance in the eventual physical interaction with humans.

Appendix A.

Normalization of the deformation

To determine the last integration constant, the normalization condition of the modes of vibrations can be exploited. The well-known proof of orthogonality of the shape functions is reported below, finally arriving at the normalization condition that can be used to determine the last coefficient of the 2.36

A.1. Orthogonality of the modes

Starting to :

$$-\frac{d^2 EI_z v''(u,t)}{du^2} = \rho A \frac{d^2 v(u,t)}{dt^2} \tag{A.1}$$

and replace $v = \chi\delta(t) = \chi e^{j\omega_i t}$ in the last equation:

$$\frac{d^2}{du^2} EI_z \chi''(u) \cancel{e^{j\omega_i t}} = \omega_i^2 \rho A \cancel{e^{j\omega_i t}}$$

Considering the "r" and "s" modes of vibrating with $r \neq s$ we have:

$$\begin{aligned} m(u) &= \rho A \\ \frac{d^2}{du^2} EI_z \chi_r''(u) &= \omega_r^2 m(u)\, \chi_r \\ \frac{d^2}{du^2} EI_z \chi_s''(u) &= \omega_s^2 m(u)\, \chi_s \end{aligned}$$

Taking the first and multiplying by the way χ_s we get:

$$\int_0^l \chi_s(u) \frac{d^2}{du^2} EI_z \chi_r''(u)\, du = \omega_r^2 \int_0^l m(u)\, \chi_s(u)\, \chi_r du \tag{A.2}$$

Taking the left member and integrating it by parts two times we obtain:

Appendix A. Normalization of the deformation

$$\chi_s(u)\frac{d}{du}EI_z\frac{d^2\chi_r(u)}{du^2}\bigg|_0^l - \frac{d\chi_s(u)}{du}EI_z\frac{d^2\chi_r(u)}{du^2}\bigg|_0^l + \int_0^l EI_z\frac{d^2\chi_s(u)}{du^2}\frac{d^2\chi_r(u)}{du^2} \tag{A.3}$$

Considering a stuck beam we have that $\chi(0) = 0\ \chi'(0) = 0$,therefore by substituting these conditions we obtain:

$$\chi_s(l)\ \underbrace{\frac{d}{du}EI_z\frac{d^2\chi_r(l)}{du^2}}_{\mathbf{T}(l)} - \frac{d\chi_s(l)}{du}\ \underbrace{EI_z\frac{d^2\chi_r(l)}{du^2}}_{\mathbf{M}(l)} + \int_0^l EI_z\frac{d^2\chi_s(u)}{du^2}\frac{d^2\chi_r(u)}{du^2}$$

Where:

- $\mathbf{T}(l)$ is the shear at the free end
- $\mathbf{M}(l)$ it's torque to the free end

Now repeating the same operation for $\chi_s(u)$ and by comparing we obtain:

$$\chi_s(l)\frac{d}{du}EI_z\frac{d^2\chi_r(l)}{du^2} - \frac{d\chi_s(l)}{dx}EI_z\frac{d^2\chi_r(l)}{du^2} + \int_0^l EI_z\frac{d^2\chi_s(u)}{du^2}\frac{d^2\chi_r(u)}{du^2} \tag{A.4}$$

$$\chi_r(l)\frac{d}{du}EI_z\frac{d^2\chi_s(l)}{du^2} - \frac{d\chi_r(l)}{du}EI_z\frac{d^2\chi_s(l)}{du^2} + \int_0^l EI_z\frac{d^2\chi_r(u)}{du^2}\frac{d^2\chi_s(u)}{du^2} \tag{A.5}$$

Considering that the shear and the torque at the free end are null and remembering the right member of the A.2 we have that:

$$\int_0^l \chi_s(u)\,\omega_r^2 m(u)\,\chi_r = \int_0^l \chi_r(u)\,\omega_s^2 m(u)\,\chi_s(u)$$

$$(\omega_r^2 - \omega_s^2)\int_0^l \chi_s(u)\,\chi_r(u)\,m(u) = 0$$

This equation, being $\omega_s \neq \omega_r$ proves that the form functions $\chi_r(u)\chi_s(u)$ they are normal to each other.

$$(\omega_r^2 - \omega_s^2)\int_0^l \chi_s(u)\,\chi_r(u)\,m(u) = 0 \qquad s \neq r \tag{A.6}$$

On the other hand, in the event that $r = s$ we have that the modal forms are equal and therefore the integral in A.6 is not null; then the integral can be set equal to one in order to normalize the last unknown coefficient during the impositions of the boundary conditions

$$\int_0^l \chi_r^2(u)\, m(u) = 1 \qquad s = r \tag{A.7}$$

Bibliography

[1] R. C. Winfrey, "Dynamics of mechanisms with elastic links," Ph.D. dissertation, U.C.L.A., 1969.

[2] ——, "Dynamic analysis of elastic link mechanisms by reduction of coordinates," *Journal of Engineering for Industry*, vol. 94, no. 2, pp. 577–581, 1972.

[3] W. J. Book, "Modeling, design, and control of flexible manipulator arms," Ph.D. dissertation, Massachusetts Institute of Technology, 1974.

[4] W. J. Book, O. Maizza-Neto, and D. E. Whitney, "Feedback control of two beam, two joint systems with distributed flexibility," 1975.

[5] W. J. Book, "Analysis of massless elastic chains with servo controlled joints," 1979.

[6] ——, "Recursive lagrangian dynamics of flexible manipulator arms," *The International Journal of Robotics Research*, vol. 3, no. 3, pp. 87–101, 1984.

[7] M. A. Scott, M. G. Gilbert, and M. E. Demeo, "Active vibration damping of the space shuttle remote manipulator system," *Journal of guidance, control, and dynamics*, vol. 16, no. 2, pp. 275–280, 1993.

[8] K. Krishnamurthy and L. Yang, "Dynamic modeling and simulation of two cooperating structurally-flexible robotic manipulators," *Robotica*, vol. 13, no. 4, pp. 375–384, 1995.

[9] X. Cyril, G. J. Jaar, and A. K. Misra, "Dynamical modelling and control of a spacecraft-mounted manipulator capturing a spinning satellite," *Acta Astronautica*, vol. 35, no. 2, pp. 167–174, 1995, astrodynamics.

[10] V. Gouliaev and T. Zavrazhina, "Dynamics of a flexible multi-link cosmic robot-manipulator," *Journal of Sound and vibration*, vol. 243, no. 4, pp. 641–657, 2001.

[11] H. Sawada, H. Ueno, M. Oda, S. Matunaga, and K. Konoue, "Input shaping experiment for damping vibration in manual operation of a large robotic arm," in *Proceedings of The 8th International Symposium on Artificial Intelligence, Robotics, and Automation in Space, Sept*, vol. 5, 2005.

[12] J. Jansen, S. March-Leuba, D. Kwon, S. Babcock, B. Burks, R. Kress, and W. Hamel, "Long-reach manipulation for waste storage tank remediation," Oak Ridge National Lab., TN (United States), Tech. Rep., 1992.

[13] R. Kress, L. Love, R. Dubey, and A. Gizelar, "Waste tank cleanup manipulator modeling and control," in *Proceedings of International Conference on Robotics and Automation*, vol. 1. IEEE, 1997, pp. 662–668.

[14] G. Dubus, O. David, and Y. Measson, "Vibration control of a flexible arm for the iter maintenance using unknown visual features from inside the vessel," in *2009 IEEE/RSJ International Conference on Intelligent Robots and Systems*, 2009, pp. 5697–5704.

[15] I.-C. Lin and L.-C. Fu, "Adaptive hybrid force/position control of a flexible manipulator for automated deburring with online cutting trajectory modification," in *Proceedings. 1998 IEEE International Conference on Robotics and Automation (Cat. No.98CH36146)*, vol. 1, 1998, pp. 818–825.

[16] L.-H. Chang and L.-C. Fu, "Nonlinear adaptive control of a flexible manipulator for automated deburring," in *Proceedings of International Conference on Robotics and Automation*, vol. 4, 1997, pp. 2844–2849.

[17] Z. Yang and J. Sadler, "A one-pass approach to dynamics of high-speed machinery through three-node lagrangian beam elements," *Mechanism and Machine Theory*, vol. 34, no. 7, pp. 995–1007, 1999.

[18] I. Imam, G. N. Sandor, and S. N. Kramer, "Deflection and stress analysis in high speed planar mechanisms with elastic links," 1973.

[19] C. M. Oakley and R. H. Cannon, "End-point control of a two-link manipulator with a very flexible forearm: Issues and experiments," in *1989 American Control Conference*. IEEE, 1989, pp. 1381–1389.

[20] A. De Luca and B. Siciliano, "Closed-form dynamic model of planar multilink lightweight robots," *IEEE Transactions on Systems, Man, and Cybernetics*, vol. 21, no. 4, pp. 826–839, 1991.

[21] ——, "Regulation of flexible arms under gravity," *IEEE Transactions on Robotics and Automation*, vol. 9, no. 4, pp. 463–467, 1993.

[22] B. Paden, D. Chen, R. Ledesma, and E. Bayo, "Exponentially stable tracking control for multijoint flexible-link manipulators," 1993.

[23] H. Asada, Z.-D. Ma, and H. Tokumaru, "Inverse dynamics of flexible robot arms: Modeling and computation for trajectory control," 1990.

[24] R. C. Winfrey, "Elastic link mechanism dynamics," 1971.

[25] D. A. Turcic and A. Midha, "Generalized equations of motion for the dynamic analysis of elastic mechanism systems," 1984.

[26] A. Gasparetto, "On the modeling of flexible-link planar mechanisms: experimental validation of an accurate dynamic model," *J. Dyn. Sys., Meas., Control*, vol. 126, no. 2, pp. 365–375, 2004.

[27] S. Briot and W. Khalil, "Recursive and symbolic calculation of the elastodynamic model of flexible parallel robots," *The International Journal of Robotics Research*, vol. 33, no. 3, pp. 469–483, 2014.

[28] X. Wang and J. K. Mills, "Dynamic modeling of a flexible-link planar parallel platform using a substructuring approach," *Mechanism and machine theory*, vol. 41, no. 6, pp. 671–687, 2006.

[29] R. Vidoni, P. Boscariol, A. Gasparetto, and M. Giovagnoni, "Kinematic and dynamic analysis of flexible-link parallel robots by means of an erls approach," in *International Design Engineering Technical Conferences and Computers and Information in Engineering Conference*, vol. 45035. American Society of Mechanical Engineers, 2012, pp. 1449–1458.

[30] M. Mahmoodi, J. K. Mills, and B. Benhabib, "Vibration modeling of parallel kinematic mechanisms (pkms) with flexible links: admissible shape functions," *Transactions of the Canadian Society for Mechanical Engineering*, vol. 39, no. 1, pp. 97–113, 2015.

[31] R. H. Cannon Jr and E. Schmitz, "Initial experiments on the end-point control of a flexible one-link robot," *The International Journal of Robotics Research*, vol. 3, no. 3, pp. 62–75, 1984.

[32] N. G. Chalhoub and A. G. Ulsoy, "Dynamic simulation of a leadscrew driven flexible robot arm and controller," 1986.

[33] M. Balas, "Feedback control of flexible systems," *IEEE Transactions on Automatic Control*, vol. 23, no. 4, pp. 673–679, 1978.

[34] S. Nagarajan and D. A. Turcic, "Lagrangian formulation of the equations of motion for elastic mechanisms with mutual dependence between rigid body and elastic motions: Part i element level equations," 1990.

[35] M. O. Tokhi, Z. Mohamed, and M. H. Shaheed, "Dynamic characterisation of a flexible manipulator system," *Robotica*, vol. 19, no. 5, pp. 571–580, 2001.

[36] R. J. Theodore and A. Ghosal, "Comparison of the assumed modes and finite element models for flexible multilink manipulators," *The International journal of robotics research*, vol. 14, no. 2, pp. 91–111, 1995.

[37] A. Kermanian, A. Kamali, and A. Taghvaeipour, "Dynamic analysis of flexible parallel robots via enhanced co-rotational and rigid finite element formulations," *Mechanism and Machine Theory*, vol. 139, pp. 144–173, 2019.

[38] L. Meirovitch, *Fundamentals of vibrations*. Waveland Press, 2010.

[39] G. Zhu, S. S. Ge, and T. H. Lee, "Simulation studies of tip tracking control of a single-link flexible robot based on a lumped model," *Robotica*, vol. 17, no. 1, pp. 71–78, 1999.

[40] W. Khalil and M. Gautier, "Modeling of mechanical systems with lumped elasticity," in *Proceedings 2000 ICRA. Millennium Conference. IEEE International Conference on Robotics and Automation. Symposia Proceedings (Cat. No. 00CH37065)*, vol. 4. IEEE, 2000, pp. 3964–3969.

[41] S. K. Dwivedy and P. Eberhard, "Dynamic analysis of flexible manipulators, a literature review," *Mechanism and machine theory*, vol. 41, no. 7, pp. 749–777, 2006.

[42] J. Selig and X. Ding, "A screw theory of timoshenko beams," *Journal of Applied Mechanics*, vol. 76, no. 3, 2009.

[43] S. Mahmoodi, S. Khadem, and M. Kokabi, "Non-linear free vibrations of kelvin–voigt visco-elastic beams," *International Journal of Mechanical Sciences*, vol. 49, no. 6, pp. 722–732, 2007.

[44] C. W. De Silva, "Dynamic beam model with internal damping rotatory inertia and shear deformation," *AIAA Journal*, vol. 14, no. 5, pp. 676–680, 1976.

[45] ——, *Vibration: fundamentals and practice*. CRC press, 2006.

[46] E. Bayo and R. Ledesma, "Augmented lagrangian and mass-orthogonal projection methods for constrained multibody dynamics," *Nonlinear dynamics*, vol. 9, no. 1, pp. 113–130, 1996.

[47] J. Wang and C. M. Gosselin, "A new approach for the dynamic analysis of parallel manipulators," *Multibody System Dynamics*, vol. 2, no. 3, pp. 317–334, 1998.

[48] M. Callegari, M.-C. Palpacelli, and M. Principi, "Dynamics modelling and control of the 3-rcc translational platform," *Mechatronics*, vol. 16, no. 10, pp. 589–605, 2006.

[49] S. Brillarelli and M.-C. Palpacelli, "Design of atestbench for validating multibody flexible modeld aimedat reducing oscillations in parallel kinematic machines withflexible links," *Proceedings of the Second International Jc-IFToMM Symposium*, 2019.